Research Paper

In vivo low-intensity magnetic pulses durably alter neocortical neuron excitability and spontaneous activity

Short title: LI-rTMS alters cortical excitability in vivo

Manon Boyer[1,2], Paul Baudin[2], Chloé Stengel[3], Antoni Valero-Cabre[3], Ann M. Lohof[1], Stéphane Charpier[2], Rachel M. Sherrard[1†*], Séverine Mahon[2†*]

[1]Sorbonne Université & CNRS, IBPS-B2A, UMR 8256 Biological Adaptation and Ageing, Paris 75005, France

[2]Sorbonne Université, Paris Brain Institute–ICM, INSERM, CNRS, APHP, Pitié-Salpêtrière Hospital, team 'Network Dynamics and cellular excitability', Paris 75013 France

[3]Sorbonne Université, Paris Brain Institute–ICM, INSERM, CNRS, Pitié-Salpêtrière Hospital, team Cerebral Dynamics, Plasticity and Rehabilitation Group, FRONTLAB team, Paris 75013, France.

*Corresponding authors:
Rachel M Sherrard
UMR 8256 B2A Biological Adaptation and Ageing
Boite 256, Sorbonne Université
9 Quai St Bernard, 75005, Paris

email: rachel.sherrard@sorbonne-universite.fr

Severine Mahon
Paris Brain Institute–ICM
INSERM U1127
Pitié-Salpêtrière Hospital, Paris 75013 France

email: severine.mahon@upmc.fr

† These authors contributed equally to this work

Abstract

Magnetic brain stimulation is a promising treatment for neurological and psychiatric disorders. However, a better understanding of its effects at the individual neuron level is essential to improve its clinical application. We combined focal low-intensity repetitive transcranial magnetic stimulation (LI-rTMS) to the rat somatosensory cortex with intracellular recordings of subjacent pyramidal neurons *in vivo*. Continuous 10 Hz LI-rTMS reliably evoked firing at ~4-5 Hz during the stimulation period and induced durable attenuation of synaptic activity and spontaneous firing in cortical neurons, through membrane hyperpolarization and a reduced intrinsic excitability. However, inducing firing in individual neurons by repeated intracellular current injection did not reproduce LI-rTMS effects on neuronal properties. These data provide novel understanding of mechanisms underlying magnetic brain stimulation showing that, in addition to inducing biochemical plasticity, even weak magnetic fields can activate neurons and enduringly modulate their excitability.

Introduction

Repetitive transcranial magnetic stimulation (rTMS) is a promising tool for the treatment of neurological and psychiatric diseases. However, a better understanding of the cellular mechanisms underlying rTMS effects is needed to optimize current treatment protocols, whose outcomes remain variable (Bhattacharya et al., 2021; Cirillo et al., 2017; Rossini et al., 2015). Clinical application of magnetic stimulation delivers repeated high-intensity (0.5–2 Tesla, T) magnetic pulses to a targeted cortical area to induce an electric field that activates cortical neurons and initiates activity-dependent plasticity (Bhattacharya et al., 2021; Cirillo et al., 2017). Such plasticity is confirmed in rodents, where high-intensity magnetic stimulation *in vitro* induces synaptic plasticity in hippocampal networks (Lenz and Vlachos, 2016; Vlachos et al., 2012) and modulates neocortical inhibitory interneurons (Hoppenrath et al., 2016; Mix et al., 2015).

Besides high-field magnetic stimulation, whose duration and frequency of application is limited by technical and safety reasons (Rossini et al., 2015), new protocols using low-intensity (milliTesla, mT) magnetic fields are emerging. Human studies show that low-intensity stimulation to the entire brain can modulate EEG activity and cerebral function (Cook et al., 2009; Di Lazzaro et al., 2013; Rohan et al., 2014). In addition, focal application of these weak stimuli (low-intensity rTMS; LI-rTMS) in rodents facilitates the reorganisation of abnormal circuits (Makowiecki et al., 2014; Rodger et al., 2012), stimulates axonal growth and synaptogenesis (Dufor et al., 2019), and modifies cellular calcium signalling and gene expression (Dufor et al., 2019; Grehl et al., 2015). However, low-intensity stimulation is thought to generate electric fields weaker than those considered able to initiate action potential (AP) firing (Chan and Nicholson, 1986; Grehl et al., 2016; Radman et al., 2009). Thus, it remains unclear how LI-rTMS alters the properties of single neurons to contribute to structural and functional changes. Moreover, human cortical responses to magnetic stimulation critically depend on the ongoing activity of the stimulated brain region (Silvanto and Pascual-Leone, 2008). It is therefore

78 necessary to identify the impact of LI-rTMS on the electrical properties of cortical neurons *in vivo*, *i.e.*
79 in a physiologically relevant experimental condition that preserves neuronal connectivity.
80
81 We developed an *in vivo* model to deliver focal low-intensity (10 mT) rTMS to the somatosensory cortex
82 (S1) of sedated rodents during intracellular recording of underlying pyramidal neurons. We provide
83 direct evidence that LI-rTMS reliably elicits action potentials (APs) in S1 pyramidal cells. Also, 10
84 minutes of continuous 10 Hz LI-rTMS produces long lasting (≥ 40 minutes post-stimulation)
85 modifications in intrinsic membrane properties and spontaneous activity. These after-effects include
86 dampening of resting membrane properties, membrane hyperpolarization, and weaker background
87 synaptic and firing activity. This was accompanied by altered transfer function, characterized by
88 increased minimal current required to induce neuronal firing. These LI-rTMS-mediated effects were not
89 reproduced by 10 minutes of AP firing, induced by intracellular injection of threshold current pulses at
90 10 Hz. Our data show that, like high-intensity stimulation, LI-rTMS activates neurons and durably
91 modulates their activity and excitability. This changes the paradigm for brain stimulation with weak
92 magnetic fields and increases the range of potentially therapeutic stimulation parameters for clinical use.
93
94
95 **Results**
96 To study the immediate and time-dependent effects of LI-rTMS on cortical activity, we paired *in vivo*
97 intracellular recordings of S1 neurons (n=41 from 31 rats) with ECoG monitoring (Fig. 1, A–C). Some
98 recorded neurons were filled with neurobiotin (n=19) and confirmed histologically as pyramidal neurons
99 located in layer 5 (n=11) or 2/3 (n=8; Fig. 1B). All recorded neurons displayed the characteristic firing
100 of S1 pyramidal cells (Mahon and Charpier, 2012; Zhu and Connors, 1999): regular spiking (n=27; Fig.
101 3B) or intrinsic bursts of APs (n=14) following suprathreshold current pulse injection (Fig. 3B, fig. S1).

102 Since no differences in LI-rTMS effects were observed between pyramidal neurons located in layers 2/3
103 or layer 5, we pooled the corresponding results.
104
105 **LI-rTMS decreases spontaneous neuronal activity**
106 First, we verified the stability of S1 cortical neuron recordings by measuring the variability of electrical
107 membrane properties for 20 minutes preceding LI-rTMS (Fig. 1C, fig. S1). During this control period,
108 the LI-rTMS coil was positioned above S1, but no stimulation was delivered. There were no significant
109 changes in neuronal spontaneous activity or membrane excitability during this baseline period (fig. S1;
110 see Supplementary Information for details). To analyze the time-dependent effects of LI-rTMS (*n*=16
111 experiments), we divided recordings into five consecutive periods: 1) pre-stimulation (Pre), the 10
112 minutes immediately before LI-rTMS; 2) 10 minutes LI-rTMS at 10 Hz; and 3) three successive post-
113 stimulation times: 10–20 min (P1), 20–30 min (P2) and 40–50 min (P3) after the start of LI-rTMS (Fig.
114 1C). Before stimulation, spontaneous intracellular activity showed broadband frequency, small
115 amplitude synaptic fluctuations, and a Gaussian-like distribution of membrane potential values (Vm)
116 around -72.1 ± 4.8 mV (mean±SD; *n*=16 neurons) (Fig. 1C Pre, Fig. 2A-B). In half of the recorded
117 neurons, background synaptic activity caused spontaneous firing at 1.8 ± 2.3 Hz (*n*=8) with high temporal
118 variability (CV2 ISIs = 1.2 ± 0.3, *n*=8) (Figs. 1C, 2A). Consistent with this intracellular activity, the
119 ECoG showed desynchronized, relatively fast, small-amplitude cortical waves (Fig. 1C), as classically
120 observed under sufentanil sedation (Altwegg-Boussac et al., 2017, 2014).
121
122 In all tested neurons, 10 minutes continuous 10 Hz LI-rTMS induced membrane hyperpolarization
123 compared to Pre (Fig. 2A-C), which was present immediately after LI-rTMS (P1: -2.3 ± 2.0 mV, *n*=16
124 neurons; $P<0.01$) and persisted until the end of recording (P3: -2.3 ± 1.9 mV, *n*=9 neurons; $P<0.01$)
125 (Figs. 1Cb, 2A-C), resulting in a negative shift of the Vm distribution during the post-stimulation periods

126 (Fig. 2B left). Background synaptic activity amplitude (Vm standard deviation) was also reduced after
127 LI-rTMS in both active and silent neurons (Fig. 2A), reaching a 10.8 ± 12.2 % decrease at P3 as compared
128 to the pre-stimulation period ($P<0.01$, $n=9$ neurons) (Fig. 2A-C). This was associated with reduced power
129 of synaptic activity for frequencies below 10 Hz (Fig. 2A, B). This dampening of synaptic noise
130 amplitude was unexpected because sustained Vm hyperpolarization should increase synaptic current
131 driving force and therefore synaptic potentials, particularly given the lack of inward membrane
132 rectification in the voltage-current (*V-I*) relationships in our recorded cells (fig. S1Bb).
133
134 Consistent with attenuated intracellular synaptic events and cell hyperpolarization, the spontaneous firing
135 of these cortical neurons was markedly reduced after LI-rTMS. Five of the 8 neurons active prior to LI-
136 rTMS became completely silent by P2, while firing of the 3 remaining cells decreased to 0.07 ± 0.13 Hz
137 at P3 (Fig. 2A-C). This failure of cell firing was not due to altered ionic AP mechanisms, as their
138 amplitude, half-width duration and threshold voltage did not change (Fig. 2B right, table S1); it more
139 likely reflected the decreased background synaptic drive.
140
141 **LI-rTMS alters neuronal integrative properties and input-output relationship**
142 We next tested if LI-rTMS altered the excitability of S1 pyramidal neurons by changing their integrative
143 properties, *i.e.* their ability to process subthreshold membrane currents, and their input-output
144 relationship before and after stimulation.
145
146 We first examined changes in membrane input resistance (Rm) and membrane time constant (τm), two
147 parameters that govern, respectively, the ability of synaptic currents to change Vm and the efficacy with
148 which a neuron summates synaptic potentials over time. Rm values, extrapolated from the slope of the
149 *V-I* curves (fig. S1B), were already significantly reduced at P1 (compared to Pre: -14.1 ± 6.6 %, n =11

150 neurons; $P<0.001$), a decrease that persisted for up to 40 min after the end of stimulation (n=9 neurons;
151 $P<0.01$) (Fig. 3A, C). The decrease in Rm was not caused by LI-rTMS-mediated changes in the
152 morphology of recorded neurons, whose anatomical properties were comparable to those classically
153 described for S1 pyramidal cells (Brecht et al., 2003; Mahon and Charpier, 2012; Manns et al., 2004)
154 (Fig. 1B). τm values also showed a persistent decrease that closely matched the reduction in Rm (Fig.
155 3C). The attenuation of Rm and τm by LI-rTMS may contribute to the smaller amplitude of spontaneous
156 synaptic potentials and their ineffective summation to elicit APs.
157
158 As changes in Vm and Rm can affect the reactivity of a neuron to its inputs (Altwegg-Boussac et al.,
159 2014; Silver, 2010), we looked for possible LI-rTMS-induced modifications in the input-output
160 relationship. We injected positive current pulses of increasing intensity during the different recording
161 periods and counted the number of evoked APs, generating frequency-current (*F-I*) curves (fig S1Cb,
162 Fig. 3B). After LI-rTMS, *F-I* curves progressively shifted to the right, leading to a ~50% increase of the
163 threshold current values by P3 (n=7 neurons; compared to Pre, $P<0.05$) (Fig. 3B, C). This reduced
164 neuronal responsiveness to small excitatory inputs was accompanied by relatively stable neuronal gain,
165 defined as the slope of the linear portion of *F-I* curves, throughout the post-stimulation period ($P = 0.23$)
166 (Fig. 3C).
167
168 **Low-intensity magnetic pulses trigger APs**
169 To identify the mechanisms initiating the long-lasting inhibitory effects of LI-rTMS on cortical activity
170 and integrative properties, we investigated the immediate effects of LI-rTMS during the stimulation
171 period. A practical difficulty arises from the brief (~1.6 ms) large-amplitude artifacts generated by each
172 LI-rTMS pulse (Figs. 1, 4, fig. S2), which obscures the early part of the neuronal response. However, we
173 noticed in all recorded neurons (n=16) that the terminal part of many artifacts was rapidly followed by a
174 biphasic voltage waveform resembling an intracellular AP (Fig. 4A, fig. S2A). We thus removed the

175 stimulation artifacts off-line from traces displaying an apparent AP waveform (see Methods, and Figs.
176 4, 5 and fig. S2 for details). The artifact-free recordings revealed intracellular waveforms whose shape,
177 peak amplitude and kinetics matched those of spontaneous APs recorded from the same neurons (Fig.
178 4Ab). The mean latency of AP-like events, calculated from the end of the stimulus to the peak of the
179 waveform, was 0.6 ± 0.1 ms (*n*=16 neurons) and the percentage of individual magnetic pulses
180 immediately preceding these waveforms was 24 ± 31 % (*n*=16 neurons; Fig 4B, bottom left), with a high
181 cell-to-cell variability (from 0.3 to 99.8 %). Given that magnetic intensity decreases by distance-squared,
182 we tested whether this inter-neuronal variability depended on the depth of recorded cells; there was no
183 correlation (r^2 = 0.03). Notably, these AP-like events are not non-biological artifacts resulting from direct
184 action of the magnetic field on the recording electrode, as they did not occur in control experiments in
185 which a model cell was used to simulate the recording of a pyramidal neuron (fig. S2B).
186
187 To confirm that the high-voltage waveforms were indeed APs, we tested their sensitivity to sustained
188 Vm hyperpolarization - which prevents firing by moving the neuron's Vm further from the AP threshold
189 - or to the blockade of voltage-gated sodium channels by the lidocaine analog QX-314. In the absence of
190 LI-rTMS, spontaneous firing frequency which was 1.8 ± 1.6 Hz at rest (Vm = -71.9 ± 7.0 mV, *n*=6 tested
191 neurons), declined with imposed *DC* hyperpolarization (from -0.1 to -2 nA), and fell to zero when Vm
192 reached -81.2 ± 8.1 mV (*n*=6 neurons) (Fig. 4B, top). Vm hyperpolarization was associated with
193 increased amplitude of synaptic fluctuations, as expected from a greater driving force of excitatory
194 synaptic currents (Fig. 4B, top right). Hyperpolarizing these same cortical neurons during short periods
195 of LI-rTMS similarly decreased the rate of the AP-like events, from 4.0 ± 2.7 Hz at rest (*n*=6 neurons)
196 to a residual rate of 0.04 ± 0.05 Hz at the most negative membrane polarization tested (Vm = -81.2 ± 8.1
197 mV, *n*=6 neurons) (Fig. 4B, bottom).
198

199 Second, to test whether the putative LI-rTMS-induced APs had the same ionic mechanisms as
200 spontaneous APs, we perfused the intracellularly recorded neurons with QX-314 (n=9) and compared
201 the drug-related changes in amplitude of both types of AP. In each neuron, measurements were made
202 during alternating control and stimulation periods of 5–160 seconds. The peak potential of spontaneous
203 APs was progressively reduced (P<0.05) by the QX314 (Fig. 4C) and this time-dependent reduction was
204 accompanied by a mean Vm depolarization of 5–10 mV, as classically observed in QX-314-filled cortical
205 neurons (Benardo et al., 1982; Connors and Prince, 1982). The decrease in peak values of LI-rTMS-
206 induced waveforms and spontaneous APs was almost identical for any given time after the onset of QX-
207 314 diffusion (P>0.2 for each recording time), reaching ~ -14–20 mV in the neurons that could be
208 recorded until 30–40 min after cell impalement (n=5) (Fig. 4C). Because the QX314-reduced APs were
209 occasionally difficult to distinguish from spontaneous depolarized synaptic potentials in recordings of
210 long duration (Fig. 4Ca, arrows), we also examined the effects of QX-314 on APs evoked by depolarizing
211 current steps (0.2–0.4 nA, n=9 neurons) (Fig. 4Cb, Cc). Again, the time-course of the reduction in
212 current-induced AP peak potentials was similar to that measured for LI-rTMS-induced APs (P>0.1 for
213 each recording time) (Fig. 4Cb, Cc).
214
215 The LI-rTMS-induced APs occurred in all recorded cortical neurons, regardless of their firing frequency
216 prior to stimulation (Fig. 5A-C). This led to a significant increase in the overall firing rate (including
217 both spontaneous and LI-rTMS-evoked APs) throughout the LI-rTMS period (n=16 neurons; P<0.05)
218 (Fig. 5B). However, the rate of spontaneous APs, when measured separately, was decreased by almost
219 45% during LI-rTMS (Pre: 1.8 ± 2.3 Hz, n=8 active neurons, LI-rTMS: 0.6 ± 0.8 Hz, n=8 neurons; P <
220 0.01) (Fig. 5B). The induced APs did not result from a LI-rTMS-mediated increase in synaptic activity
221 or sustained membrane depolarization since artifact-free records did not show significant change in the
222 amplitude of Vm fluctuations in association with the firing induced by magnetic pulses (Figs. 4, 5, and
223 fig. S2A). However, their short latency and ability to be evoked from relatively hyperpolarized membrane

224 potentials indicate that LI-rTMS-evoked APs probably resulted from activation of an axonal site located
225 close to the soma.
226
227 These results demonstrate for the first time that 10 Hz LI-rTMS can elicit AP firing in pyramidal neurons,
228 with kinetic and ionic mechanisms similar to spontaneous APs, despite inducing an electric field
229 estimated to be at least 100 times lower than that used in high-intensity rTMS. They also demonstrate
230 that 10 minutes continuous 10 Hz LI-rTMS produces robust and long-lasting inhibitory effects on the
231 activity and integrative properties of individual pyramidal neurons.
232
233 **Action potentials evoked by intracellular current injection do not reproduce LI-rTMS effects**
234 In order to determine whether the LI-rTMS-induced firing was responsible for the changes in cortical
235 neuron activity and responsiveness, we examined, in another group of S1 neurons, the impact of an AP
236 discharge evoked by intracellular injection of current steps. Single cortical neurons (n=7) were
237 challenged with repetitive depolarizing current pulse stimulation (rCPS) delivered intracellularly at10
238 Hz for 10 min (Fig. 6A). Intensity of current steps was adjusted in each neuron to obtain a proportion of
239 suprathreshold stimulations (~30%) and an overall firing frequency comparable to those produced by LI-
240 rTMS (5.9 ± 4.6 Hz, n=7 neurons, including both spontaneous and evoked APs; P>0.4) (Fig. 6B). The
241 effects of rCPS were compared to a subgroup of magnetically stimulated neurons (n=9) with similar
242 baseline membrane electrical properties, including mean Vm, spontaneous firing frequency and Rm
243 (n=9; P>0.1 for each parameter).
244
245 The first obvious difference between effects of current-evoked APs (rCPS) and LI-rTMS was that rCPS
246 did not produce neuronal hyperpolarization during the post-stimulation period (Fig. 6C, left and fig.
247 S3D). This was accompanied by stable Vm fluctuations and spontaneous firing frequency (Pre *versus*
248 post-rCPS: P>0.2 for each parameter) (fig. S3A, D). Furthermore, comparison of V-I curves before and

249 after rCPS showed no significant modification of Rm (n=6 neurons; Pre, 17.2 ± 6.9 MΩ *vs.* Post, 17.9 ±
250 7.5 MΩ; P = 0.14) or τm (n=6 neurons; Pre, 6.5 ± 1.8 ms, vs. Post, 6.3 ± 1.6 ms; P = 0.28) (Fig. 6C,
251 middle and fig. S3B, D). Finally, analysis of *F-I* curves revealed heterogeneous modification in the
252 sensitivity of cortical neurons to weak depolarizing inputs. Although average current threshold values
253 did not significantly change (P=0.4), most neurons (n=4 out of 6 tested cells) had a significantly
254 decreased firing threshold (ΔI_{th} = -0.14 ± 0.07 nA, n=4; P<0.05) following rCPS. This modulation of
255 cortical responsiveness was not accompanied by modification in the neuronal gain (P>0.4) (Fig. 6C right
256 and fig. S3C, D). Thus, the firing of single cortical neurons at a similar frequency to that induced by
257 magnetic stimulation (~ 5 Hz) is not sufficient to reproduce, on its own, the LI-rTMS-related changes in
258 neuronal excitability.
259

260 **Discussion**

261 To our knowledge, this study is the first to investigate the immediate (online) and after- (offline) effects
262 of low-intensity rTMS on the electrical properties of single neurons *in vivo*. Because rTMS-induced
263 cortical responses depend on the ongoing brain state (Gersner et al., 2011; Silvanto and Pascual-Leone,
264 2008), we used experimental conditions which retain stable background cortical activity, similar to the
265 waking state, during the long intracellular recordings (Altwegg-Boussac et al., 2014; Bruno and
266 Sakmann, 2006; Constantinople and Bruno, 2011). Our results indicate that 10 minutes continuous 10
267 Hz LI-rTMS alters the passive membrane properties of S1 pyramidal neurons, reduces their intrinsic
268 excitability and attenuates their spontaneous firing for at least 40 min. Moreover, low-intensity magnetic
269 pulses triggered APs in all recorded neurons. These findings deepen our knowledge on the cellular
270 mechanisms underlying LI-rTMS-induced plasticity and may guide the development of new stimulation
271 patterns for clinical treatment.
272

273 **LI-rTMS induces action potentials in stimulated neurons**

274 A major and unexpected finding of our study was that low intensity (10 mT) magnetic pulses elicited
275 APs in all recorded neurons (25% of pulses on average). This challenges the common assumption that
276 LI-rTMS only acts through subthreshold mechanisms because it induces electrical fields weaker than
277 those required for neuronal activation (Chan and Nicholson, 1986; Grehl et al., 2016; Radman et al.,
278 2009). Our result is however coherent with weak electric fields inducing short-latency spiking in retinal
279 ganglion cells *in vitro* (Bonmassar et al., 2012) and medium-intensity (60 mT) magnetic pulses
280 transiently activating sodium currents to facilitate AP firing in S1 pyramidal neurons (Banerjee et al.,
281 2017) in slices. The percentage of magnetic pulses initiating APs varied between cells, consistent with
282 variable pyramidal neuron sensitivity to magnetic and electric fields, depending on their location,
283 morphology and intrinsic excitability (Radman et al., 2009; Rotem and Moses, 2008) as well as
284 fluctuations in their spontaneous firing (Pasley et al., 2009).

285

286 The mechanisms underlying magnetic pulse-induced neuronal activation remain unclear. In high-
287 intensity TMS, trans-synaptic or direct neuronal depolarization are thought to initiate APs in the axon
288 (Müller-Dahlhaus and Vlachos, 2013; Pashut et al., 2014; and references therein). Here, LI-rTMS-
289 induced APs had short latency, were not associated with increased subthreshold synaptic events, and
290 could be triggered from a hyperpolarized Vm, suggesting direct activation of the axon initial segment,
291 whose high concentration of voltage-gated sodium channels confers a lower AP threshold (Eccles, 2013;
292 Kole et al., 2008).

293

294 **Continuous 10 Hz LI-rTMS durably decreases cortical excitability and activity**

295 The main after-effects of LI-rTMS included smaller amplitude background synaptic noise, substantial
296 membrane hyperpolarization and marked reduction or cessation of spontaneous firing. These changes in

297 spontaneous activity were accompanied by attenuated neuronal integrative properties (correlated
298 decrease in Rm and τm) and reduced intrinsic excitability (higher minimal current firing threshold).
299
300 The likely primary origin of these effects, whether altered synaptic events or intrinsic cellular properties,
301 can be deduced from our data. Long-term depression of synaptic inputs onto the recorded neurons, which
302 could explain the observed reduction in synaptic activity, would decrease global membrane conductance
303 (due to smaller excitatory synaptic conductance) and thus increase Rm and τm values (Destexhe et al.,
304 2003) – the opposite of our findings. Rather, we suggest that LI-rTMS-mediated inhibition of neuronal
305 activity originates from alteration to cortical neuron integrative properties. Indeed, the initial reduction
306 in Rm and τm, which attenuates neuronal responsiveness to their synaptic inputs, would explain both the
307 reduced amplitude of Vm fluctuations and membrane hyperpolarization. Given the inverse correlation
308 linking current firing threshold to Vm in cortical neurons (Altwegg-Boussac et al., 2014; Carton-Leclercq
309 et al., 2021), the membrane hyperpolarization would in turn explain the rightward shift of input-output
310 relations and the reduced intrinsic excitability. Finally, all these cellular modifications will combine to
311 reduce the efficiency with which cortical neurons process synaptic currents and generate APs and, thus,
312 explain the progressive decrease of spontaneous firing. This reduced firing in individual neurons will
313 contribute to global reduction of synaptic activity flow within the stimulated cortical network, which will
314 further reduce synaptic and firing activity. Furthermore, increased activity of neocortical GABAergic
315 interneurons could also contribute to reducing pyramidal cell activity, by producing a robust shunting
316 effect on pyramidal neuronal membrane (Tremblay et al., 2016) and lowering Rm (due to larger
317 inhibitory synaptic conductance).
318
319 The precise subcellular mechanisms through which LI-rTMS exerts its effects warrant further
320 investigation. We hypothesize that increased neuronal firing during stimulation opens voltage-gated

calcium channels, increasing intracellular calcium and activating calcium-dependent enzymatic cascades that regulate ionic conductances (Delord et al., 2007; Xu and Kang, 2005). In line with this hypothesis, pyramidal neuron firing induced by medium-intensity (60 mT) rMS *in vitro* is associated with increased cytosolic calcium (Banerjee et al., 2017). Moreover, our data showing changes in Rm and current firing threshold together with stable neuronal gain after LI-rTMS suggest that the long-lasting decrease in neuronal excitability is due to modulation of potassium currents activated around resting Vm (Naudé et al., 2012). This suggestion is supported by previous reports, in which similar depression of intrinsic cell excitability was attributed to calcium-dependent upregulation of slowly-inactivating potassium currents (Li et al., 2004; Lombardo et al., 2018).

Our results also indicate that induced APs, and their associated changes in calcium concentration, may not be sufficient to trigger the time-dependent post-LI-rTMS effects. Simply replicating the level of LI-rTMS-induced AP firing by repeated intracellular injection of current pulses in single neurons did not significantly modify resting and active membrane properties. This suggests that electric field-induction is only one of several mechanisms activated by electromagnetic pulses. We have previously shown that cryptochrome magnetoreceptors are required for neuroplasticity effects of LI-rTMS (Dufor et al., 2019) and modulate reactive oxygen species (ROS) (Sherrard et al., 2018). In cell redox physiology, ROS activate ryanodine receptors to release calcium from intracellular stores (Görlach et al., 2015), a phenomenon we have demonstrated in cortical neurons in response to LI-rTMS (Grehl et al., 2015). It is therefore likely that both voltage-gated calcium channel activation and calcium release from intracellular stores are required for the long-term modulation of pyramidal neuron activity.

Relevance of LI-rTMS to human rTMS treatment

The LI-rTMS-induced inhibitory effects on neuronal excitability and firing is surprising in light of former studies using high-intensity rTMS. According to these reports, high-frequency magnetic stimulation (≥

346 5 Hz) should increase cortical excitability (Bhattacharya et al., 2021; Cirillo et al., 2017; Huang et al.,
347 2005), potentiate excitatory synaptic transmission and/or upregulate the expression of neurochemical
348 markers of synaptic plasticity (Cirillo et al., 2017; Gersner et al., 2011; Lenz et al., 2015; Vlachos et al.,
349 2012).
350
351 However, there are important differences between those reports and our study, which can explain the
352 different outcomes. First, in some of these studies, rTMS effects on synaptic function were examined *ex*
353 *vivo* after repeated daily sessions of high-frequency rMS (Cirillo et al., 2017; Gersner et al., 2011), which
354 is not the case here. Second, in studies where acute effects of magnetic stimulation were measured, rMS
355 was usually delivered directly to a brain slice or organotypic culture and not to an intact brain as in our
356 *in vivo* experimental condition (Lenz et al., 2015; Tang et al., 2016; Vlachos et al., 2012) . For example,
357 in mouse S1 slices, 3 minutes of medium-intensity (85 mT) intermittent theta-burst magnetic stimulation
358 reduced AP voltage threshold in pyramidal neurons and increased their current-evoked firing, without
359 changing resting membrane properties (Tang et al., 2016). Discordance between results obtained *in vitro*
360 and in living brains has already been reported: opposite changes in synaptic efficacy can be induced *in*
361 *vivo* and *in vitro* at the same synapses by the same stimulation paradigm (Mahon et al., 2004). Thus
362 differences between previous observations and our current *in vivo* findings reinforce that rTMS outcomes
363 depend on ongoing activity in the targeted neural networks during the stimulation (Gersner et al., 2011;
364 Silvanto and Pascual-Leone, 2008). Finally, most previous studies used magnetic fields at least ten times
365 stronger than the one used in our study. High-intensity, high-frequency stimulation protocols require
366 regular pauses to allow the coil to cool – resulting in short periods (a few seconds) of stimulation
367 separated by pauses without stimulation (see Bhattacharya et al., 2021; Cirillo et al., 2017 for reviews),
368 an intermittent pattern in contrast to our continuous 10 Hz. Theta-burst stimulation, for example, induces
369 opposite effects if applied continuously versus intermittently (Huang et al., 2005). Thus, LI-rTMS effects

370 on cell excitability are likely to depend on stimulation parameters, similar to the pattern-dependence of
371 LI-rTMS effects on structural and biochemical plasticity (Dufor et al., 2019; Grehl et al., 2015).
372
373 Although the functional consequences of LI-rTMS-mediated depression of cortical excitability for S1
374 network function and behavior remain unknown, our LI-rTMS protocol could be useful in epileptic
375 disorders, which are often associated with cortical hyperexcitability and paroxysmal network
376 synchronization (Kimiskidis et al., 2014). An understanding of the immediate and lasting effects on
377 neuronal activity, measured in real time, is an important advance for the development and evaluation of
378 stimulation patterns in future clinical treatments.
379
380 In summary, our findings that even weak magnetic fields can activate neurons and modulate their
381 excitability, change our understanding of low-intensity magnetic brain stimulation. We show that low-
382 intensity approaches have some underlying processes in common with already established high-intensity
383 clinical treatments, but without the constraints of special high-voltage equipment. This knowledge not
384 only expands the range of stimulation protocols (pulse frequency and patterns), and therefore future
385 potential clinical treatments, but also renders LI-rTMS treatments available beyond the hospital setting.
386
387
388 **Materials and Methods**
389 **Animals, their preparation and surgery**
390 All animal experiments received approval (APAFIS no. 18003-2019051019017280) from the *Charles*
391 *Darwin* Animal Experimentation Ethics Committee (C2EA-05), in accordance with the guidelines of the
392 European Union (directive 2010/603/EU). Experiments were conducted *in vivo* on adult Sprague Dawley
393 rats (n = 31) of either sex (Charles River Laboratories, France). Under isoflurane (3.5%; Centravet,
394 France) anesthesia, animals underwent tracheotomy for artificial ventilation (room air, 85 breaths.min^{-1},

395 2.6 ml.cycle^{-1}) under neuromuscular blockade (gallamine triethiodide, 40 mg/2h i.m; Sigma-Aldrich,
396 France). They were placed in a stereotaxic frame and small craniotomies were made above the left barrel
397 field of S1 (1.2–1.3 mm posterior to bregma, 4.1–6.5 mm lateral to midline; Paxinos and Watson, 1986)
398 to allow simultaneous recording of ECoG and intracellular activity of subjacent pyramidal neurons. After
399 craniotomy, isoflurane was discontinued, but sedation and analgesia were maintained by repeated
400 injection of sufentanil (3 µg/kg every 30 min, i.p.; Piramal) and local infiltration of lidocaine (2%,
401 Centravet) in incision and pressure points. Sedation with sufentanil (Niemegeers et al., 1976) was chosen
402 because it induces a globally stable background ECoG activity characterized by low amplitude
403 desynchronized cortical waves resembling those encountered during the waking state (Altwegg-Boussac
404 et al., 2017, 2014; Bruno and Sakmann, 2006; Constantinople and Bruno, 2011; Depaulis et al., 2016).
405 It thus avoids anesthesia-related modulation of cortical responses to magnetic stimulation, as observed
406 in both animal and human studies (Gersner et al., 2011; Silvanto and Pascual-Leone, 2008). Physiological
407 parameters were continuously monitored during recordings (Altwegg-Boussac et al., 2017; Schramm et
408 al., 2020). Each animal formed its own control, with LI-rTMS effects compared to baseline
409 measurements obtained before the magnetic stimulation. After the recordings, animals were euthanized
410 with euthasol (40%, i.p.; Centravet) for histological examination (see below).
411

412 ***In vivo* multi-scale electrophysiological recordings**

413 Intracellular recordings were performed with glass micropipettes filled with 2-M potassium acetate (50-
414 90 MΩ). Current-clamp recordings were amplified using an Axoclamp 900A amplifier (Molecular
415 Devices, Union City, CA, USA) operating in bridge mode, filtered between *DC* and 30 kHz and digitized
416 at 10 kHz (CED 1401plus, Spike2 software version 7.06; Cambridge Electronic Design). Intracellularly
417 recorded neurons (n = 41), identified as pyramidal cells by their morphological and electrophysiological
418 characteristics (Steriade, 2004), were located in layers 2/3 and 5 at depths ranging between 800–3300
419 µm below the cortical surface (Paxinos and Watson, 1986; Wilent and Contreras, 2004). In some

420 experiments (n = 8), we added to the pipette solution 50–100 mM of QX-314 (Tocris Biosciences), a
421 voltage-gated sodium channels blocker known to suppress APs in a time-dependent manner (Connors
422 and Prince, 1982; Wilson and Kawaguchi, 1996).
423 Spontaneous ECoG activity was recorded with a low-impedance (~60 kΩ) silver electrode placed on the
424 dura above S1 and a reference electrode placed on a contralateral temporal muscle. Surface cortical
425 signals were amplified using a differential *AC* amplifier (Model 1700; A-M Systems), filtered at 1 Hz–
426 1 kHz, and digitized at 3 kHz.
427

428 **Stimulation protocols**

429 Continuous 10Hz LI-rTMS was applied for 10 minutes (6000 pulses) using a miniaturized round coil
430 connected to an electromagnetic pulse generator (E-Lab5, Global Energy Medicine, Perth, Australia),
431 which generated 300-µs monophasic pulses of 10mT intensity, as previously described (Makowiecki et
432 al., 2014; Rodger et al., 2012). The coil was secured to a micromanipulator and placed above S1 (Fig.
433 1A). Brain-to-coil distance was minimized (~2 mm) while assuring contact-free stimulation
434 perpendicular to the cortical surface. We verified that LI-rTMS caused no electromagnetic interference
435 in the recording leads and electrodes, with negative control experiments in which a model cell (CLAMP-
436 1U Model Cell, Molecular Devices, Union City, USA) in 'cell mode' was attached to the headstage
437 amplifier (fig. S2B).
438 Repetitive current pulse stimulation consisted of intracellular injections of depolarizing square current
439 pulses (40 ms of duration) at 10 Hz for 10 min. The intensity of the current pulses (0.1–0.5 nA) was
440 adjusted for each neuron to evoke an AP every 3–5 current pulses, mimicking the frequency of LI-rTMS-
441 induced APs.
442

443 **Intracellular and ECoG signal analysis**

444 Spontaneous activity, membrane excitability and integrative properties of cortical neurons were assessed
445 before and after LI-rTMS. Average membrane potential (Vm) was calculated as the mean of the
446 distribution of spontaneous subthreshold membrane potential values and the magnitude of Vm
447 fluctuations was quantified as the standard deviation (σ) of the distribution (σVm). Time-frequency maps
448 illustrating the spectral content of synaptic activity over time were constructed using a multitaper
449 decomposition analysis with a sliding time window of 3 seconds (Oostenveld et al., 2011), after removing
450 APs which were replaced by a piecewise cubic hermite polynomial interpolation. Power spectra were
451 computed by averaging the time-frequency decomposition over a 10-minute period.
452 Mean spontaneous firing rate and Vm values were measured from recordings of at least 1 min. The
453 regularity of neuronal firing was calculated by the CV2 method: here $CV2 = (2|\Delta t_{i+1} - \Delta t_i|)/(\Delta t_{i+1} + \Delta t_i)$,
454 and $\Delta t_i = t_i - t_{i-1}$ is the inter-spike-interval (Altwegg-Boussac et al., 2014). AP properties were measured
455 from spontaneously occurring APs. AP voltage threshold was defined as the Vm at which $dVm.dt^{-1}$ first
456 exceeds 10 $mV.ms^{-1}$ (Mahon and Charpier, 2012). AP amplitude was calculated from threshold to peak
457 potential and AP half-width was the duration of the waveform at half-amplitude.
458 Dynamic changes of Vm, σVm and spontaneous firing frequency were assessed over successive windows
459 of 30 seconds. Recording periods during which cortical excitability was assessed (see below) were
460 removed from this analysis and replaced by a linear interpolation.
461 Rm was calculated as the slope of the linear portion of voltage-current (*V-I*) plots generated following
462 repeated injections of hyperpolarizing current of increasing intensity (200 ms at 2 Hz, 10–20 trials per
463 intensity, -0.2 to -0.8 nA) or from the average voltage deflection induced by hyperpolarizing current
464 pulses of -0.4 nA (200 ms, ≥ 10 trials). τm was derived from an exponential decay fit applied to the initial
465 phase of the mean current-induced hyperpolarization. Neuronal transfer function (*F–I* relationship),
466 which describes the cell output firing as a function of injected depolarizing current pulses of increasing
467 intensity (200 ms at 2 Hz, 10–20 trials per intensity, 0.1–1.5 nA), was quantified before and after LI-

468 rTMS. Linear regression of *F–I* curves yielded the threshold current for AP generation (I_{th}; *x*-intercept)
469 and neuronal gain (γ; slope) (Altwegg-Boussac et al., 2014; Mahon and Charpier, 2012).
470

471 **LI-rTMS artifact removal**

472 To assess changes in cortical activity during the 10 minutes of LI-rTMS, we removed brief high-
473 amplitude electrical artifacts induced by the magnetic pulses. We removed the recorded signal for 1.6 ms
474 following each pulse onset and preserved continuity by linear interpolation (fig. S2), as described for
475 human stimulation experiments (Amengual et al., 2017; Stengel et al., 2021). We validated this approach,
476 by adding a new channel containing artificially generated stimulation events at 10 Hz for 10 minutes to
477 control recordings. These false artifacts were then removed with the same procedure and the resulting
478 electrophysiological signal compared to the original to ensure their similarity (Amengual et al., 2017).
479

480 **Neuronal labelling**

481 Neurons were filled with neurobiotin (1.5% in the pipette solution; Vector Laboratories, Burlingame,
482 USA) through repeated depolarizing current pulse injections over 10 minutes after the end of the post-
483 stimulation period, as previously described (Mahon and Charpier, 2012). Rats were euthanized with
484 euthasol and transcardially perfused with 0.3% glutaraldehyde-4% paraformaldehyde in PBS (0.1 M,
485 pH 7.4; VWR Chemicals, France), and the neurobiotin-filled neurons revealed as previously described
486 (Williams et al., 2016).
487

488 **Statistical analysis**

489 Data were explored for normality, outliers and statistical test assumptions in Prism version 9.00
490 (GraphPad Inc., San Diego, USA). Group differences were assessed using paired two-tailed Student's t-
491 test, one-way Repeated Measures ANOVA, or non-parametric Wilcoxon signed rank test and the Mann-
492 Whitney rank sum test. The Benjamini-Hochberg test was used to correct for multiple comparisons

493 (Benjamini and Hochberg, 1995). Values are expressed as means ± SD and significance level was $P <$

494 0.05.

495

496

References

Altwegg-Boussac T, Chavez M, Mahon S, Charpier S. 2014. Excitability and responsiveness of rat barrel cortex neurons in the presence and absence of spontaneous synaptic activity in vivo. *J Physiol* **592**:3577–3595. doi:10.1113/jphysiol.2013.270561

Altwegg-Boussac T, Schramm AE, Ballestero J, Grosselin F, Chavez M, Lecas S, Baulac M, Naccache L, Demeret S, Navarro V, Mahon S, Charpier S. 2017. Cortical neurons and networks are dormant but fully responsive during isoelectric brain state. *Brain* **140**:2381–2398. doi:10.1093/brain/awx175

Amengual JL, Vernet M, Adam C, Valero-Cabré A. 2017. Local entrainment of oscillatory activity induced by direct brain stimulation in humans. *Sci Rep* **7**:41908. doi:10.1038/srep41908

Banerjee J, Sorrell ME, Celnik PA, Pell G. 2017. Immediate Effects of Repetitive Magnetic Stimulation on Single Cortical Pyramidal Neurons. *PloS One* **12**:e0170528. doi:10.1371/journal.pone.0170528

Benardo LS, Masukawa LM, Prince DA. 1982. Electrophysiology of isolated hippocampal pyramidal dendrites. *J Neurosci* **2**:1614–1622.

Benjamini Y, Hochberg Y. 1995. Controlling the False Discovery Rate: A Practical and Powerful Approach to Multiple Testing. *J R Stat Soc Ser B Methodol* **57**:289–300.

Bhattacharya A, Mrudula K, Sreepada SS, Sathyaprabha TN, Pal PK, Chen R, Udupa K. 2021. An Overview of Noninvasive Brain Stimulation: Basic Principles and Clinical Applications. *Can J Neurol Sci* **48:**1–14. doi:10.1017/cjn.2021.158

Bonmassar G, Lee SW, Freeman DK, Polasek M, Fried SI, Gale JT. 2012. Microscopic magnetic stimulation of neural tissue. *Nat Commun* **3**:921. doi:10.1038/ncomms1914

Brecht M, Roth A, Sakmann B. 2003. Dynamic receptive fields of reconstructed pyramidal cells in layers 3 and 2 of rat somatosensory barrel cortex. *J Physiol* **553**:243–265. doi:10.1113/jphysiol.2003.044222

Bruno RM, Sakmann B. 2006. Cortex is driven by weak but synchronously active thalamocortical synapses. *Science* **312**:1622–1627. doi:10.1126/science.1124593

Carton-Leclercq A, Lecas S, Chavez M, Charpier S, Mahon S. 2021. Neuronal excitability and sensory responsiveness in the thalamo-cortical network in a novel rat model of isoelectric brain state. *J Physiol* **599**:609–629. doi:10.1113/JP280266

Chan CY, Nicholson C. 1986. Modulation by applied electric fields of Purkinje and stellate cell activity in the isolated turtle cerebellum. *J Physiol* **371**:89–114.

Cirillo G, Di Pino G, Capone F, Ranieri F, Florio L, Todisco V, Tedeschi G, Funke K, Di Lazzaro V. 2017. Neurobiological after-effects of non-invasive brain stimulation. *Brain Stimulat* **10**:1–18. doi:10.1016/j.brs.2016.11.009

Connors BW, Prince DA. 1982. Effects of local anesthetic QX-314 on the membrane properties of hippocampal pyramidal neurons. *J Pharmacol Exp Ther* **220**:476–481.

Constantinople CM, Bruno RM. 2011. Effects and mechanisms of wakefulness on local cortical networks. *Neuron* **69**:1061–1068. doi:10.1016/j.neuron.2011.02.040

Cook CM, Saucier DM, Thomas AW, Prato FS. 2009. Changes in human EEG alpha activity following exposure to two different pulsed magnetic field sequences. *Bioelectromagnetics* **30**:9–20. doi:10.1002/bem.20434

Delord B, Berry H, Guigon E, Genet S. 2007. A new principle for information storage in an enzymatic pathway model. *PLoS Comput Biol* **3**:e124. doi:10.1371/journal.pcbi.0030124

Depaulis A, David O, Charpier S. 2016. The genetic absence epilepsy rat from Strasbourg as a model to decipher the neuronal and network mechanisms of generalized idiopathic epilepsies. *J Neurosci Methods* **260**:159–174. doi:10.1016/j.jneumeth.2015.05.022

Destexhe A, Rudolph M, Paré D. 2003. The high-conductance state of neocortical neurons in vivo. *Nat Rev Neurosci* **4**:739–751. doi:10.1038/nrn1198

Di Lazzaro V, Capone F, Apollonio F, Borea PA, Cadossi R, Fassina L, Grassi C, Liberti M, Paffi A,

546 Parazzini M, Varani K, Ravazzani P. 2013. A consensus panel review of central nervous system
547 effects of the exposure to low-intensity extremely low-frequency magnetic fields. *Brain Stimulat*
548 **6**:469–476. doi:10.1016/j.brs.2013.01.004
549 Dufor T, Grehl S, Tang AD, Doulazmi M, Traoré M, Debray N, Dubacq C, Deng Z-D, Mariani J, Lohof
550 AM, Sherrard RM. 2019. Neural circuit repair by low-intensity magnetic stimulation requires
551 cellular magnetoreceptors and specific stimulation patterns. *Sci Adv* **5**:eaav9847.
552 doi:10.1126/sciadv.aav9847
553 Eccles JC. 2013. The Physiology of Synapses. Academic Press.
554 Gersner R, Kravetz E, Feil J, Pell G, Zangen A. 2011. Long-Term Effects of Repetitive Transcranial
555 Magnetic Stimulation on Markers for Neuroplasticity: Differential Outcomes in Anesthetized and
556 Awake Animals. *J Neurosci* **31**:7521. doi:10.1523/JNEUROSCI.6751-10.2011
557 Görlach A, Bertram K, Hudecova S, Krizanova O. 2015. Calcium and ROS: A mutual interplay. *Redox*
558 *Biol* **6**:260–271. doi:10.1016/j.redox.2015.08.010
559 Grehl S, Martina D, Goyenvalle C, Deng Z-D, Rodger J, Sherrard RM. 2016. In vitro Magnetic
560 Stimulation: A Simple Stimulation Device to Deliver Defined Low Intensity Electromagnetic
561 Fields. *Front Neural Circuits* **10**:85. doi:10.3389/fncir.2016.00085
562 Grehl S, Viola HM, Fuller-Carter PI, Carter KW, Dunlop SA, Hool LC, Sherrard RM, Rodger J. 2015.
563 Cellular and molecular changes to cortical neurons following low intensity repetitive magnetic
564 stimulation at different frequencies. *Brain Stimulat* **8**:114–123. doi:10.1016/j.brs.2014.09.012
565 Hoppenrath K, Härtig W, Funke K. 2016. Intermittent Theta-Burst Transcranial Magnetic Stimulation
566 Alters Electrical Properties of Fast-Spiking Neocortical Interneurons in an Age-Dependent
567 Fashion. *Front Neural Circuits*. **10**:22. doi:10.3389/fncir.2016.00022
568 Huang Y-Z, Edwards MJ, Rounis E, Bhatia KP, Rothwell JC. 2005. Theta burst stimulation of the human
569 motor cortex. *Neuron* **45**:201–206. doi:10.1016/j.neuron.2004.12.033
570 Kimiskidis VK, Valentin A, Kälviäinen R. 2014. Transcranial magnetic stimulation for the diagnosis and
571 treatment of epilepsy. *Curr Opin Neurol* **27**:236–241. doi:10.1097/WCO.0000000000000071
572 Kole MHP, Ilschner SU, Kampa BM, Williams SR, Ruben PC, Stuart GJ. 2008. Action potential
573 generation requires a high sodium channel density in the axon initial segment. *Nat Neurosci*
574 **11**:178–186. doi:10.1038/nn2040
575 Lenz M, Platschek S, Priesemann V, Becker D, Willems LM, Ziemann U, Deller T, Müller-Dahlhaus F,
576 Jedlicka P, Vlachos A. 2015. Repetitive magnetic stimulation induces plasticity of excitatory
577 postsynapses on proximal dendrites of cultured mouse CA1 pyramidal neurons. *Brain Struct Funct*
578 **220**:3323–3337. doi:10.1007/s00429-014-0859-9
579 Lenz M, Vlachos A. 2016. Releasing the Cortical Brake by Non-Invasive Electromagnetic Stimulation?
580 rTMS Induces LTD of GABAergic Neurotransmission. *Front Neural Circuits* **10**:96.
581 doi:10.3389/fncir.2016.00096
582 Li C, Lu J, Wu C, Duan S, Poo M. 2004. Bidirectional modification of presynaptic neuronal excitability
583 accompanying spike timing-dependent synaptic plasticity. *Neuron* **41**:257–268.
584 doi:10.1016/s0896-6273(03)00847-x
585 Lombardo J, Sun J, Harrington MA. 2018. Rapid activity-dependent modulation of the intrinsic
586 excitability through up-regulation of KCNQ/Kv7 channel function in neonatal spinal motoneurons.
587 *PloS One* **13**:e0193948. doi:10.1371/journal.pone.0193948
588 Mahon S, Charpier S. 2012. Bidirectional plasticity of intrinsic excitability controls sensory inputs
589 efficiency in layer 5 barrel cortex neurons in vivo. *J Neurosci* **32**:11377–11389.
590 doi:10.1523/JNEUROSCI.0415-12.2012
591 Mahon S, Deniau J-M, Charpier S. 2004. Corticostriatal plasticity: life after the depression. *Trends*
592 *Neurosci* **27**:460–467. doi:10.1016/j.tins.2004.06.010
593 Makowiecki K, Harvey AR, Sherrard RM, Rodger J. 2014. Low-intensity repetitive transcranial
594 magnetic stimulation improves abnormal visual cortical circuit topography and upregulates BDNF

in mice. *J Neurosci* **34**:10780–10792. doi:10.1523/JNEUROSCI.0723-14.2014

Manns ID, Sakmann B, Brecht M. 2004. Sub- and suprathreshold receptive field properties of pyramidal neurones in layers 5A and 5B of rat somatosensory barrel cortex. *J Physiol* **556**:601–622. doi:10.1113/jphysiol.2003.053132

Mix A, Hoppenrath K, Funke K. 2015. Reduction in cortical parvalbumin expression due to intermittent theta-burst stimulation correlates with maturation of the perineuronal nets in young rats. *Dev Neurobiol*. **75**:1-11. doi:10.1002/dneu.22205

Müller-Dahlhaus F, Vlachos A. 2013. Unraveling the cellular and molecular mechanisms of repetitive magnetic stimulation. *Front Mol Neurosci* **6**:50. doi:10.3389/fnmol.2013.00050

Naudé J, Paz JT, Berry H, Delord B. 2012. A theory of rate coding control by intrinsic plasticity effects. *PLoS Comput Biol* **8**:e1002349. doi:10.1371/journal.pcbi.1002349

Niemegeers CJ, Schellekens KH, Van Bever WF, Janssen PA. 1976. Sufentanil, a very potent and extremely safe intravenous morphine-like compound in mice, rats and dogs. *Arzneimittelforschung* **26**:1551–1556.

Oostenveld R, Fries P, Maris E, Schoffelen J-M. 2011. FieldTrip: Open source software for advanced analysis of MEG, EEG, and invasive electrophysiological data. *Comput Intell Neurosci* **2011**:156869. doi:10.1155/2011/156869

Pashut T, Magidov D, Ben-Porat H, Wolfus S, Friedman A, Perel E, Lavidor M, Bar-Gad I, Yeshurun Y, Korngreen A. 2014. Patch-clamp recordings of rat neurons from acute brain slices of the somatosensory cortex during magnetic stimulation. *Front Cell Neurosci* **8**:145. doi:10.3389/fncel.2014.00145

Pasley BN, Allen EA, Freeman RD. 2009. State-dependent variability of neuronal responses to transcranial magnetic stimulation of the visual cortex. *Neuron* **62**:291–303. doi:10.1016/j.neuron.2009.03.012

Paxinos G, Watson C. 1986. The Rat Brain in Stereotaxic Coordinates: Hard Cover Edition. Elsevier.

Radman T, Ramos RL, Brumberg JC, Bikson M. 2009. Role of cortical cell type and morphology in subthreshold and suprathreshold uniform electric field stimulation in vitro. *Brain Stimulat* **2**:215–228, 228.e1–3. doi:10.1016/j.brs.2009.03.007

Rodger J, Mo C, Wilks T, Dunlop SA, Sherrard RM. 2012. Transcranial pulsed magnetic field stimulation facilitates reorganization of abnormal neural circuits and corrects behavioral deficits without disrupting normal connectivity. *FASEB J* **26**:1593–1606. doi:10.1096/fj.11-194878

Rohan ML, Yamamoto RT, Ravichandran CT, Cayetano KR, Morales OG, Olson DP, Vitaliano G, Paul SM, Cohen BM. 2014. Rapid mood-elevating effects of low field magnetic stimulation in depression. *Biol Psychiatry* **76**:186–193. doi:10.1016/j.biopsych.2013.10.024

Rossini PM, Burke D, Chen R, Cohen LG, Daskalakis Z, Di Iorio R, Di Lazzaro V, Ferreri F, Fitzgerald PB, George MS, Hallett M, Lefaucheur JP, Langguth B, Matsumoto H, Miniussi C, Nitsche MA, Pascual-Leone A, Paulus W, Rossi S, Rothwell JC, Siebner HR, Ugawa Y, Walsh V, Ziemann U. 2015. Non-invasive electrical and magnetic stimulation of the brain, spinal cord, roots and peripheral nerves: Basic principles and procedures for routine clinical and research application: An updated report from an I.F.C.N. Committee. *Clin Neurophysiol.* **126:**1071-1107. doi:10.1016/j.clinph.2015.02.001

Rotem A, Moses E. 2008. Magnetic stimulation of one-dimensional neuronal cultures. *Biophys J* **94**:5065–5078. doi:10.1529/biophysj.107.125708

Schramm AE, Carton-Leclercq A, Diallo S, Navarro V, Chavez M, Mahon S, Charpier S. 2020. Identifying neuronal correlates of dying and resuscitation in a model of reversible brain anoxia. *Prog Neurobiol* **185**:101733. doi:10.1016/j.pneurobio.2019.101733

Sherrard RM, Morellini N, Jourdan N, El-Esawi M, Arthaut L-D, Niessner C, Rouyer F, Klarsfeld A, Doulazmi M, Witczak J, d'Harlingue A, Mariani J, Mclure I, Martino CF, Ahmad M. 2018. Low-intensity electromagnetic fields induce human cryptochrome to modulate intracellular reactive

644 oxygen species. *PLoS Biol* **16**:e2006229. doi:10.1371/journal.pbio.2006229
645 Silvanto J, Pascual-Leone A. 2008. State-dependency of transcranial magnetic stimulation. *Brain Topogr*
646 **21**:1–10. doi:10.1007/s10548-008-0067-0
647 Silver RA. 2010. Neuronal arithmetic. *Nat Rev Neurosci* **11**:474–489. doi:10.1038/nrn2864
648 Stengel C, Vernet M, Amengual JL, Valero-Cabré A. 2021. Causal modulation of right
649 hemisphere fronto-parietal phase synchrony with Transcranial Magnetic Stimulation during a
650 conscious visual detection task. *Sci Rep* **11**:3807. doi:10.1038/s41598-020-79812-y
651 Steriade M. 2004. Neocortical cell classes are flexible entities. *Nat Rev Neurosci* **5**:121–134.
652 doi:10.1038/nrn1325
653 Tang AD, Hong I, Boddington LJ, Garrett AR, Etherington S, Reynolds JNJ, Rodger J. 2016. Low-
654 intensity repetitive magnetic stimulation lowers action potential threshold and increases spike
655 firing in layer 5 pyramidal neurons in vitro. *Neuroscience* **335**:64–71.
656 doi:10.1016/j.neuroscience.2016.08.030
657 Tremblay R, Lee S, Rudy B. 2016. GABAergic Interneurons in the Neocortex: From Cellular Properties
658 to Circuits. *Neuron* **91**:260–292. doi:10.1016/j.neuron.2016.06.033
659 Vlachos A, Muller-Dahlhaus F, Rosskopp J, Lenz M, Ziemann U, Deller T. 2012. Repetitive Magnetic
660 Stimulation Induces Functional and Structural Plasticity of Excitatory Postsynapses in Mouse
661 Organotypic Hippocampal Slice Cultures. *J Neurosci*. doi:10.1523/JNEUROSCI.0409-12.2012
662 Wilent WB, Contreras D. 2004. Synaptic responses to whisker deflections in rat barrel cortex as a
663 function of cortical layer and stimulus intensity. *J Neurosci* **24**:3985–3998.
664 doi:10.1523/JNEUROSCI.5782-03.2004
665 Williams MS, Altwegg-Boussac T, Chavez M, Lecas S, Mahon S, Charpier S. 2016. Integrative
666 properties and transfer function of cortical neurons initiating absence seizures in a rat genetic
667 model. *J Physiol* **594**:6733–6751. doi:10.1113/JP272162
668 Wilson CJ, Kawaguchi Y. 1996. The origins of two-state spontaneous membrane potential fluctuations
669 of neostriatal spiny neurons. *J Neurosci* **16**:2397–2410.
670 Xu J, Kang J. 2005. The mechanisms and functions of activity-dependent long-term potentiation of
671 intrinsic excitability. *Rev Neurosci* **16**:311–323. doi:10.1515/revneuro.2005.16.4.311
672 Zhu JJ, Connors BW. 1999. Intrinsic firing patterns and whisker-evoked synaptic responses of neurons
673 in the rat barrel cortex. *J Neurophysiol* **81**:1171–1183. doi:10.1152/jn.1999.81.3.1171
674
675

Acknowledgments

The authors thank Sarah Lecas for histological processing and all the technical staff from the Histomics core facility of the Paris Brain Institute. Rats were housed in the PHENO-ICMice core facility, which is supported by 2 Investissements d'Avenir (ANR-10-IAIHU-06 and ANR-11-INBS-0011-NeurATRIS) and the Fondation pour la Recherche Médicale.

Funding:

Agence nationale de la recherche, ANR-19-CE37-0021
Agence nationale de la recherche, ANR-10-IAIHU-06
Agence nationale de la recherche, ANR-16-CE37-0021
Fondation Recherche Alzheimer, (MB scholarship)

Author contributions:

Conceptualization: SM, RS, SC, AL, AVC
Methodology: MB, SM, SC, RS, AL, AVC
Investigation: MB
Data analysis: MB, PB, CS, SM, RS
Supervision: SM, RS, SC, AL, AVC
Writing – original draft: SM, SC, RS, AL
Writing – review & editing: SM, SC, RS, AL, MB, PB, AVC, CS

Competing interests: Authors declare that they have no competing interests.

Data and materials availability: All data are available in the main text or the supplementary materials.

Figures and Legends

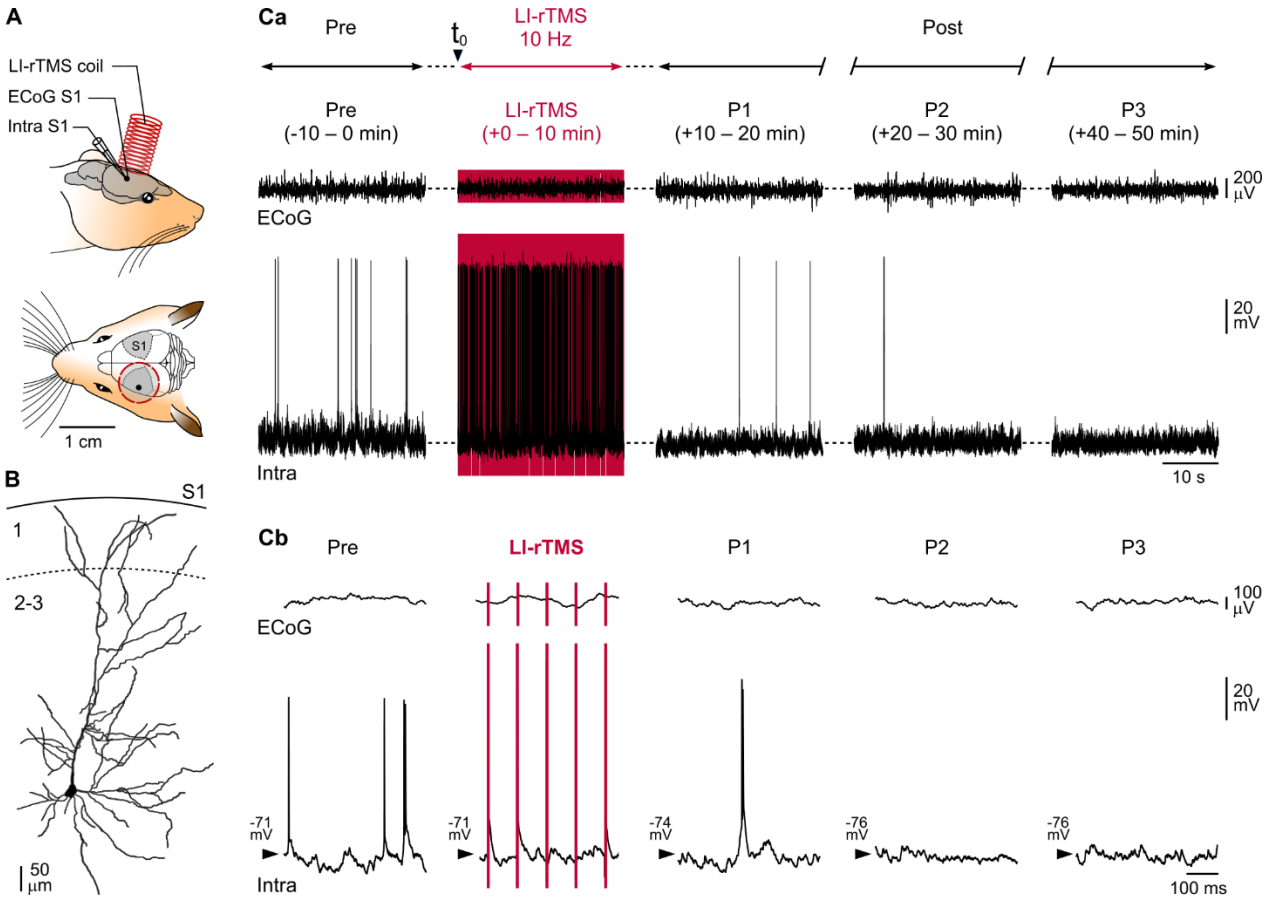

Fig. 1. Experimental paradigm and definition of recording periods.

(**A**) The experimental set-up illustrating the positions of the LI-rTMS coil and the ECoG (ECoG S1) and intracellular (Intra S1) recording electrodes. LI-rTMS (10 Hz for 10 minutes) was delivered through an 8-mm coil placed ~2 mm above the brain surface. **(B)** Reconstruction of a layer 2/3 neurobiotin-filled pyramidal neuron **(Ca)** Simultaneous ECoG and intracellular recordings from a layer 2/3 pyramidal neuron, before (Pre), during LI-rTMS, and at different times (+10−20 min, P1; +20−30 min, P2; +40−50 min, P3) after the onset of LI-rTMS (Post). **(Cb)** Expanded view (500 ms) of the recordings shown in **(Ca)**. The LI-rTMS artifacts are shown in red. Here and in the following figures, the Vm is indicated at the left of intracellular recordings.

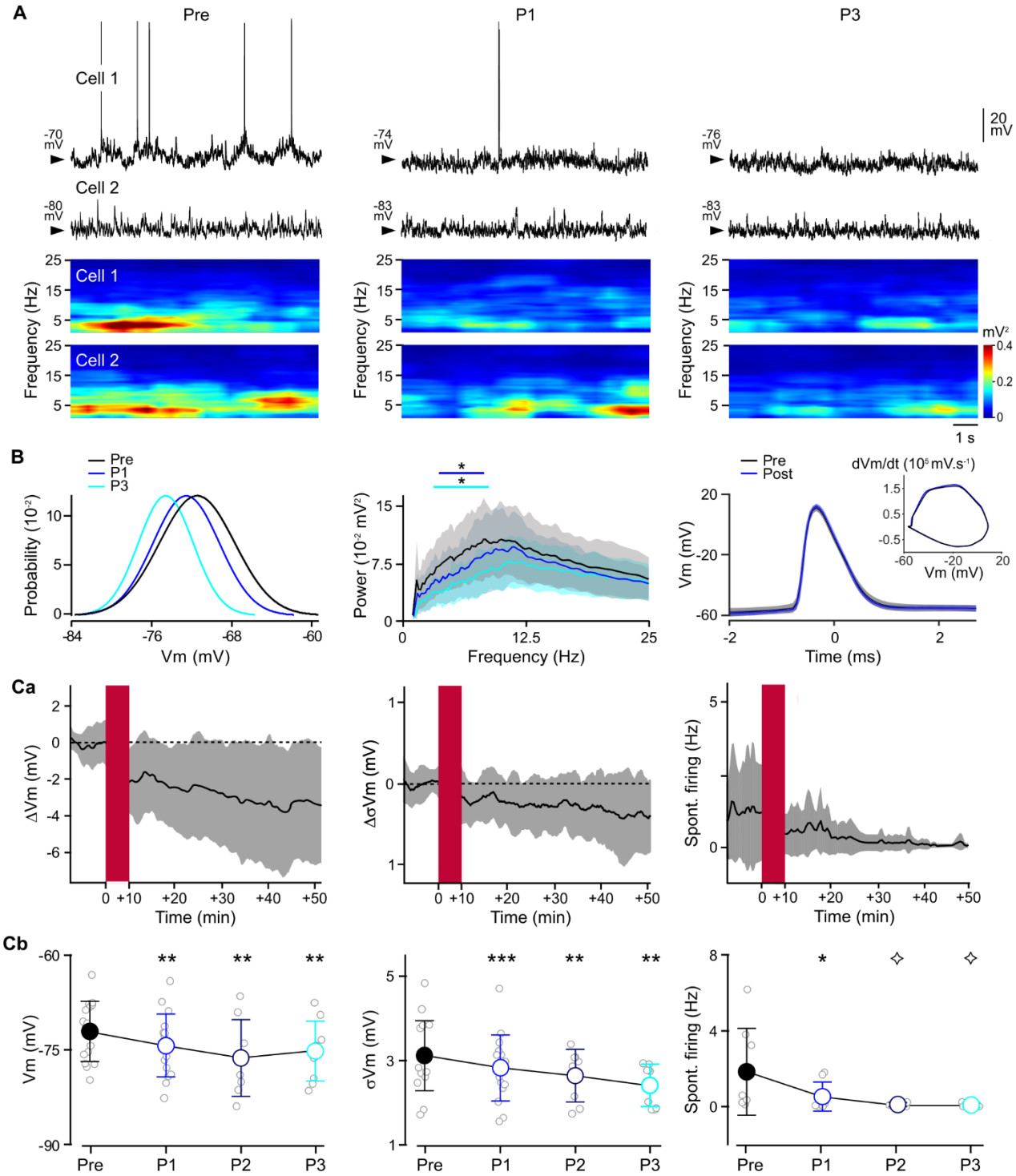

Fig. 2. LI-rTMS reduces cortical neuron spontaneous activity.

(**A**) Spontaneous intracellular activity recorded from active (cell 1) and silent (cell 2) S1 neurons before LI-rTMS (Pre) and during the first (P1) and third (P3) post-stimulation periods. The associated time-

722 frequency maps, after removal and interpolation of APs, are temporally-aligned below the records. (**B**)
723 Left: probability densities of Vm values computed from cell 2 during the different periods (60 sec of
724 recording, bin size 1 mV). Middle: mean (solid lines) ± SD (shaded areas) frequency power spectra
725 computed from intracellular subthreshold signals in the pre- and post-stimulation periods (n = 16
726 neurons) showing a progressive decrease in the power of the 5-10 Hz frequency band after LI-rTMS
727 (Wilcoxon signed rank test with Benjamini-Hochberg's post hoc correction, comparing P1 and P3 with
728 Pre). Right: superimposed examples of average ± SD (shaded areas) of spontaneous APs and
729 corresponding phase-plots (inset) during Pre (black trace, n = 138) and Post (blue trace, n = 28) periods.
730 **(C)** Time-dependent changes in spontaneous activity after 10 minutes LI-rTMS. **(Ca)** Time course of the
731 mean change (black line) ± SD (gray shaded area) in Vm (after subtraction of the mean Pre value), in the
732 amplitude of Vm fluctuation (σVm; after subtraction of the mean Pre value), and in the spontaneous
733 firing frequency of active neurons (Spont. Firing), calculated over successive 30-second periods before
734 and after LI-rTMS application (red rectangle). **(Cb)** Comparison of Vm, σVm and spontaneous firing
735 rate values (mean ± SD) during baseline (Pre) and at the three post-LI-rTMS times (P1, P2, P3)
736 [RMANOVA and Bonferroni post-hoc comparisons; Vm: n = 16, 16, 8 and 9, $F_{0.39,\ 3.89} = 12.35$, P =
737 0.034; σVm: n = 16, 16, 8 and 9, $F_{1.36,\ 13.55} = 11.69$, $P = 0.0025$; spontaneous firing: n = 8, 8, 3 and 3,
738 $F_{1.64,\ 6.03} = 9.74$, $P = 0.015$]. Here and in the following figures, the gray circles in the pooled-data graphs
739 indicate values for individual neurons. In (Ca) and (Cb), analysis of ongoing firing was restricted to
740 neurons which were spontaneously active during baseline. *$P < 0.05$, ** $P < 0.01$, *** $P < 0.001$, ns:
741 non-significant; ◊ = too few data for post-hoc comparison.
742

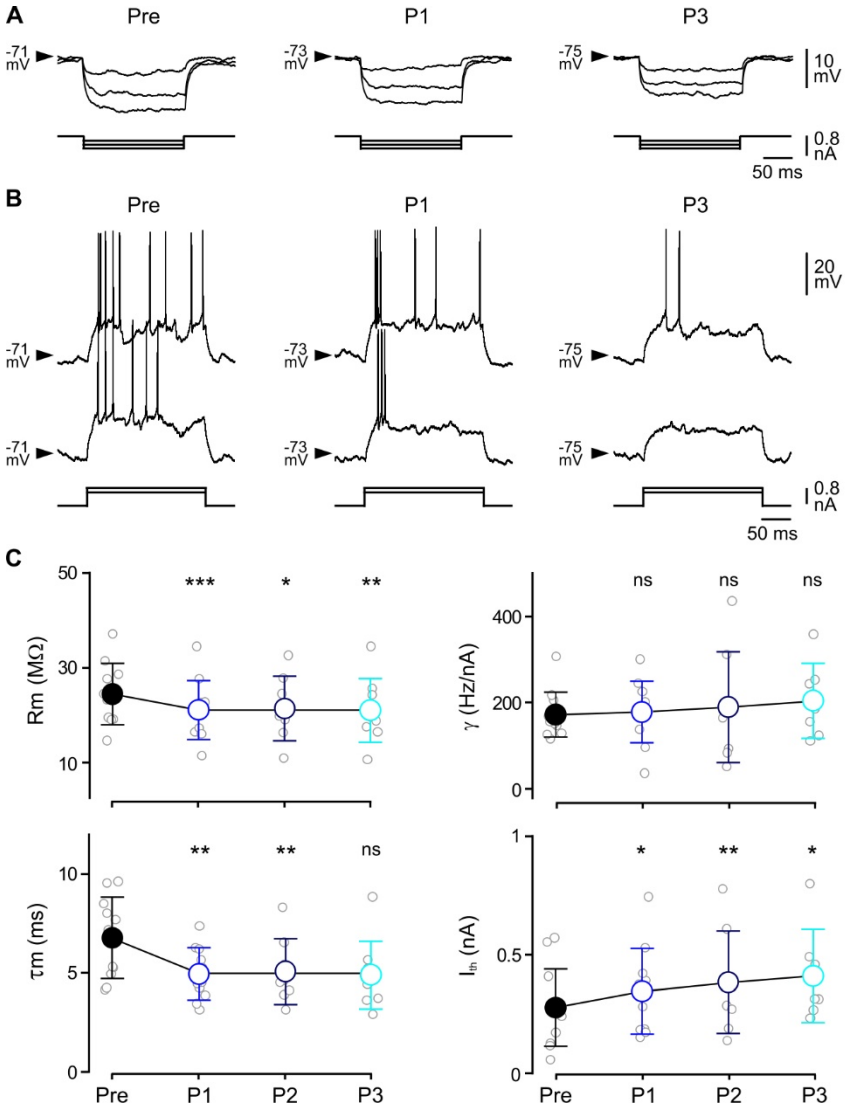

743

744 **Fig. 3. LI-rTMS negatively alters resting integrative properties and intrinsic excitability.**

745 (**A**) Average (*n* = 6–30 trials) voltage responses (upper traces) of an S1 pyramidal neuron to
746 hyperpolarizing current steps of increasing intensity (-0.2 to -0.6 nA, lower traces) before (Pre) and after
747 LI-rTMS (P1, P3). (**B**) Current-evoked firing responses of an S1 neuron to depolarizing current pulses
748 of increasing intensity during Pre, P1 and P3. (**C**) Population data showing the temporal evolution of
749 mean (± SD) values of Rm, τm, current threshold (I_{th}) and neuronal gain (γ) values. [RMANOVA and
750 Bonferroni post-hoc comparisons; Rm: *n* = 11, 11, 8 and 9, $F_{0.14, 1.19} = 10.54$, $P = 0.08$; τm: *n* = 11, 11, 8
751 and 9, $F_{1.61, 13.44} = 8.24$, $P = 0.006$; I_{th}: *n* = 12, 11, 8 and 7, $F_{0.72, 5.55} = 16.91$, $P = 0.01$; γ: *n* = 12, 11, 8 and
752 7, $F_{0.14, 1.11} = 0.66$, ns]. *$P < 0.05$, ** $P < 0.01$, *** $P < 0.001$, ns: non-significant.

753

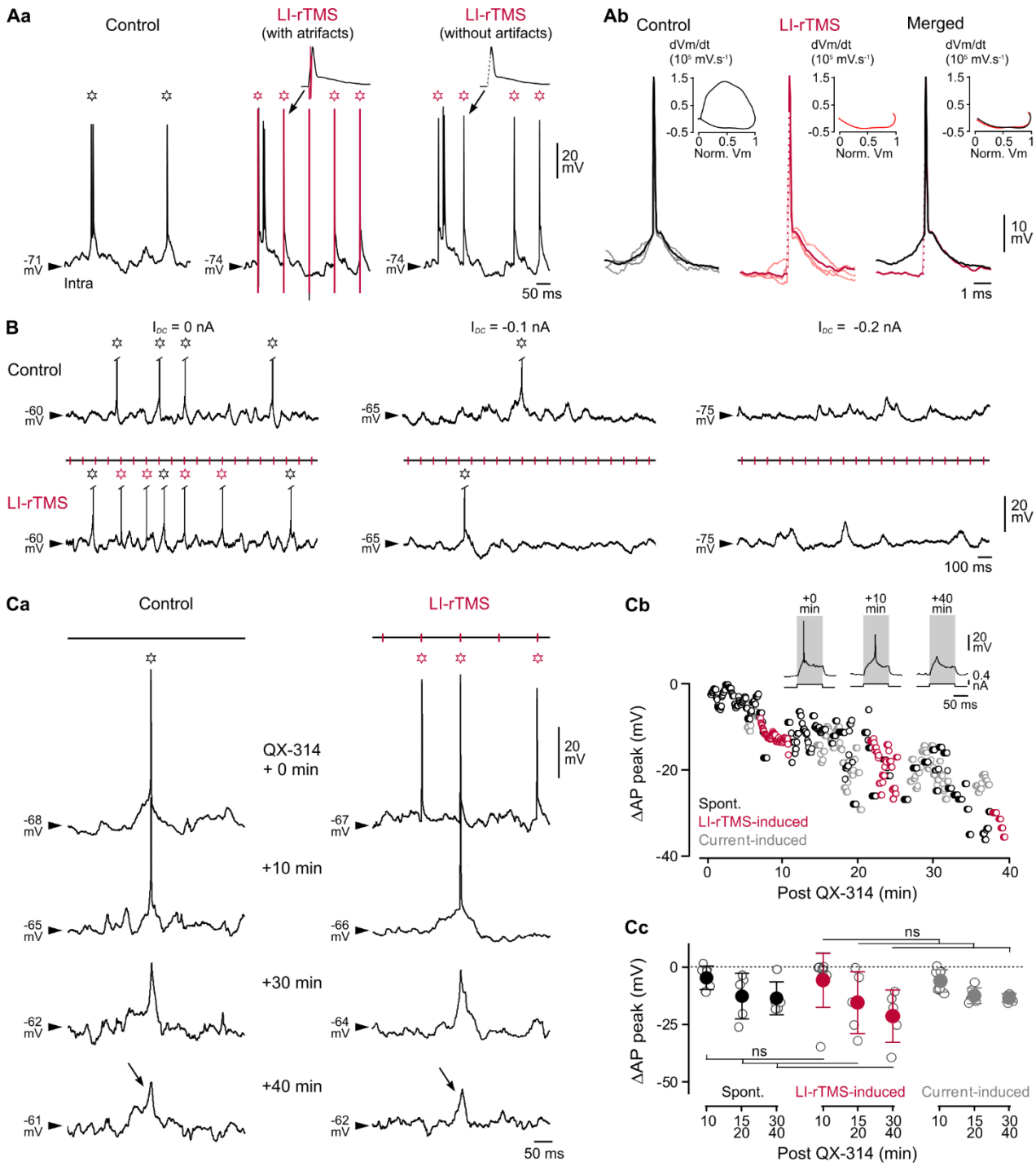

754

755 **Fig. 4. Evidence for LI-rTMS-induced APs.**

756 **(A)** Comparison of spontaneous and LI-rTMS-induced APs. **(Aa)** Intracellular activity of an S1
757 pyramidal neuron in control and during LI-rTMS, before (with artifacts, vertical red lines) and after
758 (without artifacts) removal of stimulation artifacts. Here and in the following panels, open stars mark the
759 occurrence of spontaneous (black) and putative LI-rTMS-evoked (red) APs. A typical example of a
760 putative LI-rTMS-evoked AP, with and without artifact, is enlarged above the records. Note that the

depolarizing phase of the LI-rTMS-evoked AP is hidden within the artifact. **(Ab)** *S*uperimposition of 3 spontaneous (black) or LI-rTMS-induced (red) APs (light-colored traces) with their corresponding average waveform (deeper-colored traces). The AP amplitude is normalized and LI-rTMS artifacts are indicated by dotted red lines. Note the similarity in the repolarization phase of spontaneous and LI-rTMS-induced APs when average waveforms are merged (right). The insets show the corresponding AP phase-plots (with only the repolarization phase illustrated for LI-rTMS induced APs). **(B)** Spontaneous and LI-rTMS-induced APs are blocked by membrane hyperpolarization. Cortical intracellular activity in absence of (Control, top traces) and during LI-rTMS (bottom traces) at rest (left panel) and during membrane hyperpolarization induced by intracellular injection of negative *DC*-current (middle and right panels). Red vertical markers above the traces indicate the position of the removed artifacts. **(C)** AP blockade by QX-314 in control and during LI-rTMS. **(Ca)** Examples of intracellular records obtained in absence of (left) and during (right) LI-rTMS at the indicated times after impalement with a microelectrode containing 100 mM QX-314. Times after impalement are indicated between each set of traces. Note the progressive decrease in amplitude of both spontaneous and LI-rTMS-triggered APs, which start to resemble sharp synaptic depolarizations at 30–40 min after onset of QX-314 diffusion (arrows). **(Cb)** Changes in peak potential value of individual spontaneous (black), LI-rTMS-induced (red) and current-induced (gray) APs in an S1 neuron, as a function of time after onset of QX-314 diffusion. The peak value of the first AP in each group, measured just after cell impalement, was taken as reference and artificially set to zero mV. Insets show representative current-evoked responses at the indicated times after cell impalement. **(Cc)** Pooled data comparing the peak potential decrease of spontaneous (black), LI-rTMS-induced (red) and current-induced (gray) APs at different times after QX-314 diffusion onset. [Mixed Effects ANOVA; Spont: n = 7, 5, 5 neurons; LI-rTMS-induced: n = 8, 5, 5 neurons; Current-induced: n = 8, 6, 5. Effect of time, $F_{1.21, 9,72}$ = 16,64, P = 0.0017; Effect of stimulation, $F_{1.33, 10,64}$ = 20.13 P = 0.0006). Between groups ANOVA: t0, $F_{2, 24}$ = 2.34; t10, $F_{2, 20}$ = 1.56; t15-20, $F_{2, 13}$ = 0.68; t30-40, $F_{2, 12}$ = 1.81. At each time-point, all comparisons, ns]. ns: non-significant.

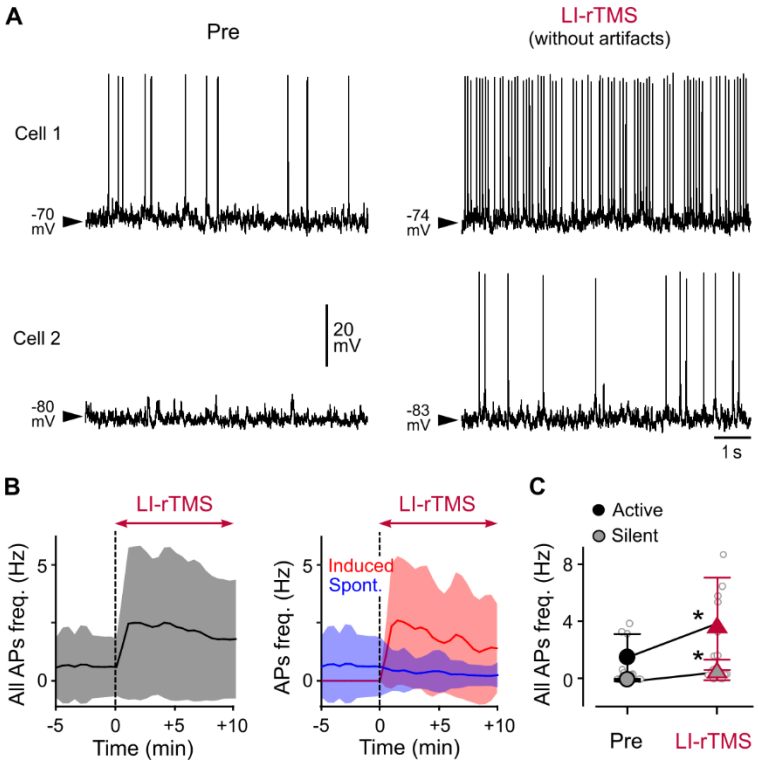

Fig. 5. Changes in firing rate during LI-rTMS.

(A) Intracellular activity of representative active (Cell 1, located in layer 2/3) and silent (Cell 2, located in layer 5) cortical neurons recorded before (Pre) and during LI-rTMS after artifact removal. **(B)** Time course of the mean (± SD, $n = 16$ neurons) changes in global firing frequency (including both spontaneous and LI-rTMS-induced APs; left) and of the specific rate of spontaneous (blue line) and TMS-mediated (red line) APs (right), calculated over 30-second periods before and during LI-rTMS (red arrow). **(C)** Summary plot comparing the mean (± SD) total AP frequency in Pre and LI-rTMS periods, separating cells that were active (black circles) and silent (gray circles) during baseline. [$n = 8$ active and 7 silent neurons, Wilcoxon Signed Rank test, $^*P < 0.05$].

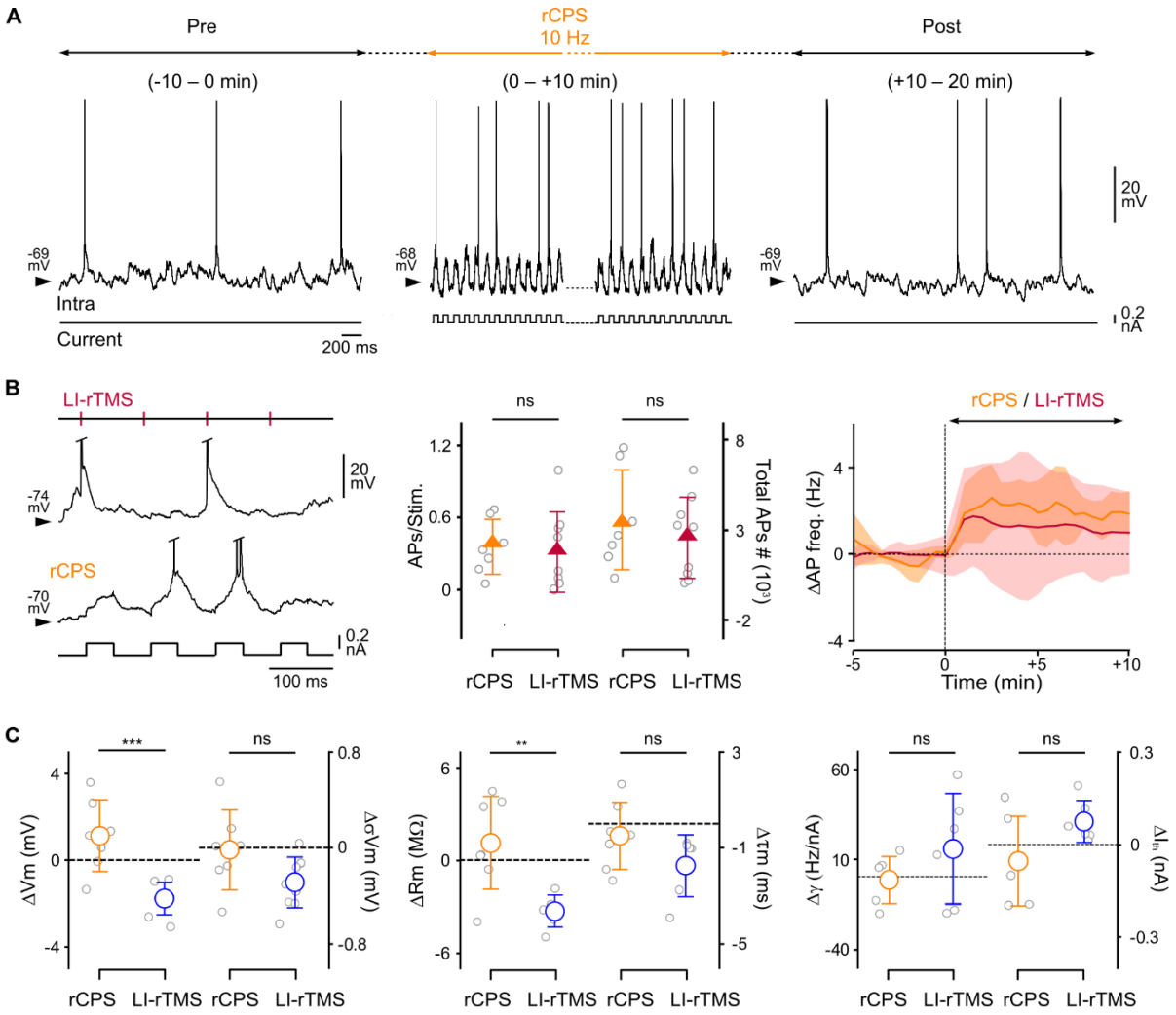

Fig. 6. Repetitive current-evoked firing in a single cortical neuron does not reproduce LI-rTMS effects

(A) Cortical intracellular activity before, during and after application of repetitive current pulse stimulation (rCPS). The rCPS protocol consisted of injecting a series of depolarizing current pulses (0.2 nA, 40 ms duration) at 10 Hz for 10 min (lower trace). **(B)** Comparison of neuronal firing during rCPS and LI-rTMS protocols. Left: Short periods of intracellular activity during LI-rTMS (top trace) and rCPS (bottom trace) paradigms. Onset times of removed LI-rTMS artifacts are indicated by red vertical markers and the timing of depolarizing current pulses is shown below the bottom trace. Middle: Pooled data comparing the mean (± SD) number of APs/stim. evoked by LI-rTMS or current pulses, and the total number of APs (evoked and spontaneous) measured over the whole stimulation period in response to rCPS (n = 7 neurons, orange triangles) or LI-rTMS (n = 9 neurons, red triangles). Right: Time course of the mean change (solid lines, n = 7 neurons) ± SD (shaded areas) in AP frequency (after subtraction of the mean Pre value) calculated over successive 30-second periods, before and during rCPS (orange)

or LI-rTMS (red) protocols. Dotted line indicates the mean Pre value, artificially set to zero. **(C)** Summary data comparing the changes in Vm, σVm, Rm, τm, γ and Ith values between pre- and post-stimulation periods after application of rCPS (orange circles) or LI-rTMS (blue circles) protocols. Dashed lines indicate the mean pre-stimulation value (Pre), artificially set to zero [Vm: n = 7, 8; σVm: n = 7, 9, Rm: n = 7, 6; γ: n = 7, 6; Ith: n = 7, 6; unpaired Student t-test; and τm: n = 7, 6; Mann Whitney Rank Sum test; ** $P < 0.01$, *** $P < 0.001$, ns: non-significant].

Supplementary Materials

Figures S1-S3
Table S1

Supplementary Materials for

In vivo low-intensity magnetic pulses durably alter neocortical neuronal excitability and spontaneous activity

Manon Boyer, Paul Baudin, Chloé Stengel, Antoni Valero-Cabré, Ann Lohof[1], Stéphane Charpier, Rachel M Sherrard[†]*, Séverine Mahon[†*]

*Corresponding authors:
Rachel M Sherrard; rachel.sherrard@sorbonne-universite.fr
Séverine Mahon ; severine.mahon@upmc.fr

This PDF file includes:

Figs. S1 to S3
Table S1

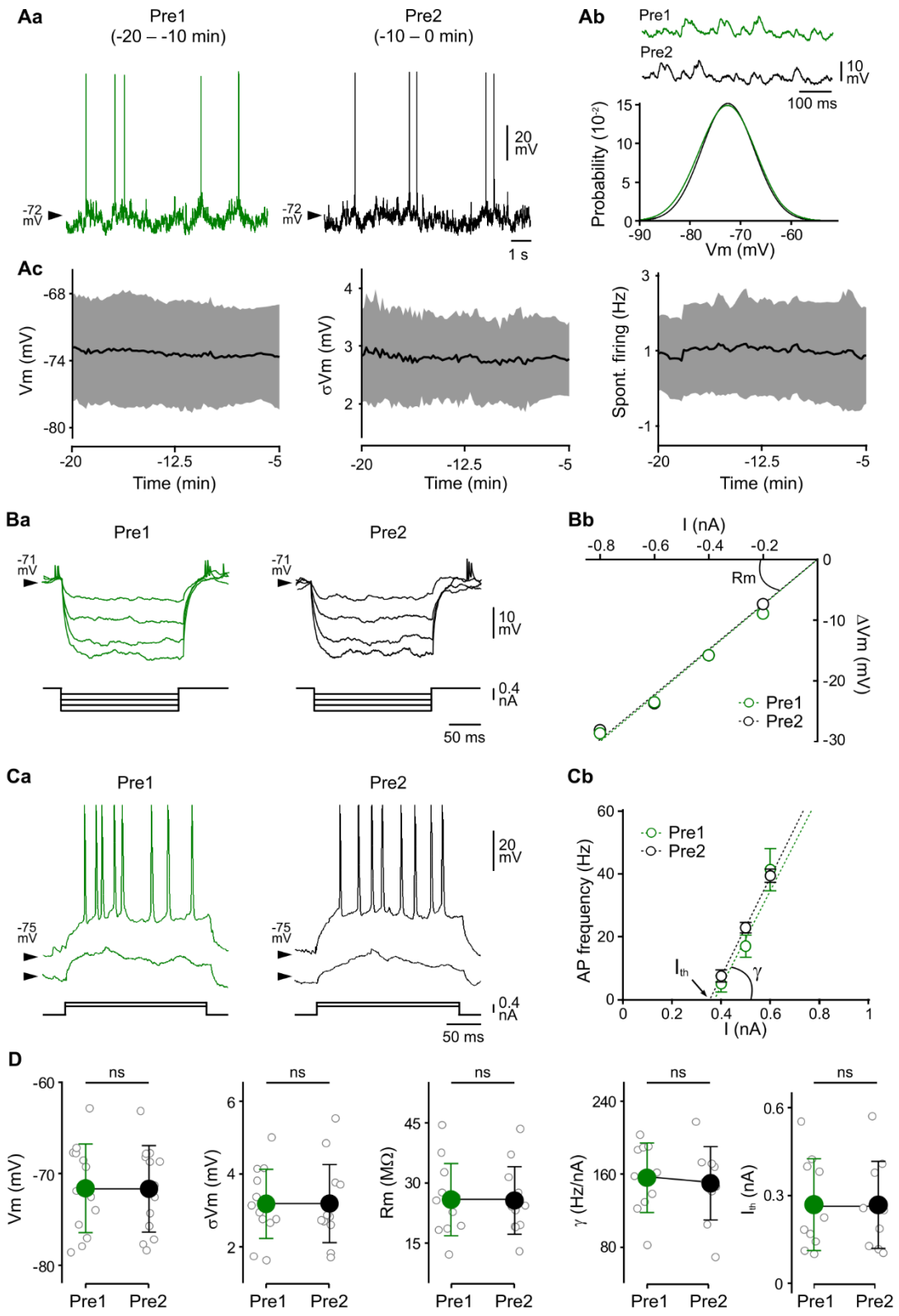
Aa
Pre1
(-20 – -10 min)
Pre2
(-10 – 0 min)
20 mV
-72 mV
1 s
Ab
Pre1
Pre2
10 mV
100 ms
Probability (10⁻²)
Vm (mV)
Ac
Vm (mV)
σVm (mV)
Spont. firing (Hz)
Time (min)
Ba
Pre1
Pre2
-71 mV
10 mV
0.4 nA
50 ms
Bb
I (nA)
Rm
ΔVm (mV)
Pre1
Pre2
Ca
Pre1
Pre2
-75 mV
20 mV
0.4 nA
50 ms
Cb
AP frequency (Hz)
I (nA)
Ith
γ
Pre1
Pre2
D
ns
Vm (mV)
σVm (mV)
Rm (MΩ)
γ (Hz/nA)
Ith (nA)
Pre1
Pre2

Fig. S1. Stability of resting integrative properties and intrinsic excitability of cortical neurons over baseline periods.

(Aa) Spontaneous intracellular activity of an S1 neuron recorded for two successive periods of 10 minutes: between 20–10 min (green trace, Pre1) and 10–0 min (black trace, Pre2) before the onset of the 10 min 10 Hz LI-rTMS protocol. Neuronal activity was characterized by a barrage of small-amplitude, broadband frequency, synaptic fluctuations (see also Fig. 2, A and B), confirming that sufentanil sedation induced cortical dynamics comparable to those observed during the waking state (Bruno and Sakmann, 2006; Constantinople and Bruno, 2011; Altwegg-Boussac et al., 2014). This background synaptic activity induced firing in 7 out of 13 neurons. Spontaneous firing rate of the active neurons was 2.9 ± 3.5 Hz during the first and 2.8 ± 3.5 Hz during the second pre-stimulation period (paired Student t-test, P = 0.29). Vm values are indicated at the left of intracellular records. **(Ab)** The probability densities of Vm values (60 s of recording, bin size 1 mV) demonstrate stability in the amplitude of synaptic activity over time. (Pre1 Vm = -71.6 ± 4.9 mV, n = 13 neurons *versus* Pre2 Vm, -71.7 ± 4.7 mV, n = 13 neurons; paired Student t-test, P = 0.92). **(Ac)** Time course of the mean values (solid lines, n = 8 neurons) ± SD (gray shaded areas) of Vm, σVm and spontaneous firing frequency computed over successive 30-second epochs during the 15 minutes of recording preceding LI-rTMS onset. Pearson's correlations indicate a lack of significant changes over time. **(B)** Stability of membrane input resistance. **(Ba)** Average (n = 10–17 trials) voltage responses (top traces) to negative current pulses of increasing intensity (bottom traces) recorded from an S1 pyramidal neuron during the two baseline periods (green traces, Pre1 and black traces, Pre2). The corresponding *V–I* relationships shown in **(Bb)** were best fitted by linear regressions (dashed lines, both $r^2 > 0.99$), indicating a lack of substantial membrane rectification in the hyperpolarizing direction. **(C)** Constancy of cell intrinsic excitability over the pre-stimulation period. **(Ca)** Examples of current-induced firing responses to depolarizing current steps of increasing intensity recorded during the two successive baseline periods (green traces, Pre1; black traces, Pre2). **(Cb)** *F-I* relationships and corresponding linear fits for the neuron illustrated in **(Ca)**. Each data point is the mean (±SD) firing rate calculated from 10–18 successive trials. **(D)** Population data comparing Vm, σVm, Rm, γ and I_{th} values during the two successive baseline periods. Gray circles correspond to values of individual neurons and green and black symbols show the mean ± SD. [Vm: n = 13; σVm: n = 13; Rm: n = 12; γ: n = 10; Ith: n = 10; paired Student t-test; *$P < 0.05$, *** $P < 0.001$, ns: non-significant].

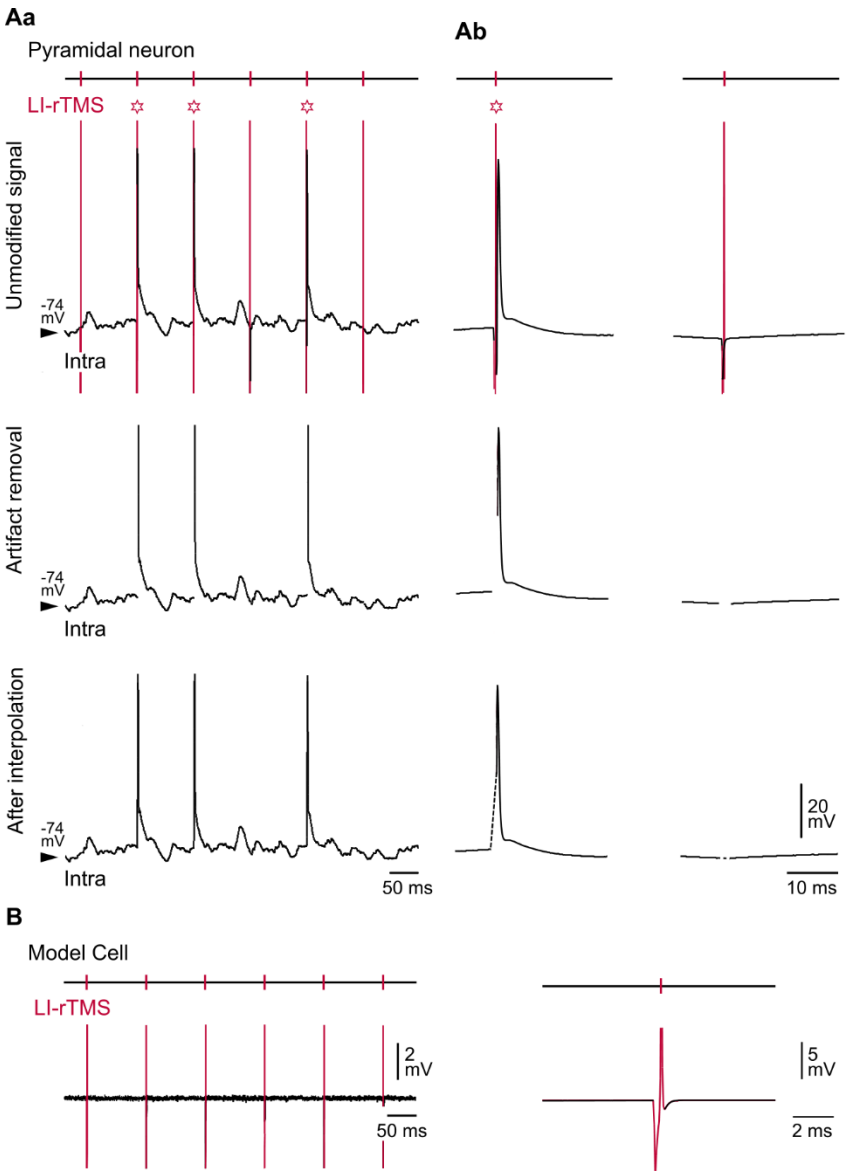

Fig. S2. Procedure for removing LI-rTMS artifacts.

(A) Off-line cutting and interpolation of electrical artifacts. **(Aa)** Short periods of intracellular activity recorded from a layer 2/3 pyramidal neuron during LI-rTMS, before removal of stimulation artifacts (vertical red lines, Unmodified signal), after their removal (Artifact removal), and after their replacement by linear interpolation (After interpolation). Red stars mark the onset of LI-rTMS-induced AP occurrences. Vm values are indicated at the left of the records. **(Ab)** Left, Representative example of an averaged (n = 2800) LI-rTMS-induced AP before and after removal of the LI-rTMS pulse stimulation artifact. Right, average cell responses (n = 3200) to magnetic pulses in absence of evoked APs. **(B)** Current-clamp recording during LI-rTMS illustrating the

absence of evoked electrical responses in the aftermath of stimulation artifacts (in red) when a CLAMP-1U model cell is simulating the recording of a pyramidal neuron. An expanded view of a single stimulation is shown at right.

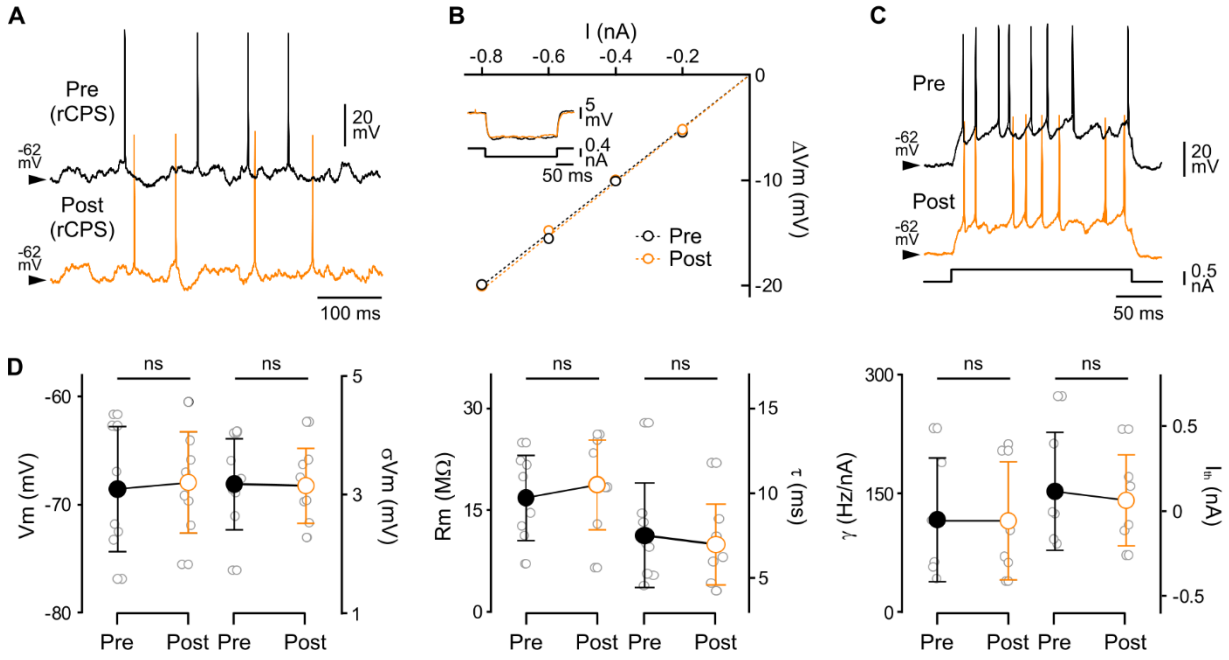

Fig. S3. Stability of neuronal resting integrative properties and intrinsic excitability after rCPS.

(**A**) Spontaneous intracellular activity recorded from an S1 neuron before (black trace, Pre) and 15 min after (orange trace, Post) the onset of the rCPS protocol. Vm values are indicated at the left of intracellular records. (**B**) *V–I* relationships computed from the neuron illustrated in (A) before and following the application of the rCPS protocol. The average voltage responses (20–30 trials) to negative current pulses of -0.4 nA (200 ms duration) during pre- and post-stimulation periods are superimposed in the inset. *V–I* relationships were best fitted by linear regressions (dashed colored lines, $r^2 > 0.99$). (**C**) Examples of current-evoked firing responses in baseline (Pre) and following rCPS (Post). (**D**) Population data comparing Vm, σVm, Rm, τm, γ and I_{th} values during the pre- and post-rCPS periods. Gray circles correspond to values of individual neurons and black and orange symbols show the mean ± SD. [Vm: $n = 7$; σVm: $n = 7$; Rm: $n = 6$; τm: $n = 6$; γ: $n = 6$; Ith: $n = 6$; paired Student t-test, ns: non-significant].

	Threshold (mV)	**Amplitude (mV)**	**Duration at mi-amplitude (ms)**	**Peak amplitude (mV)**
Pre (-10 – 0 min.)	-52.2 ± 1.1	59.7 ± 4.6	0.66 ± 0.2	7.5 ± 4.9
P1 (+10 – +20 min.)	-52.5 ± 2.2	59.2 ± 5.0	0.67 ± 0.2	6.4 ± 4.9

Table S1: Properties of spontaneous APs are similar before and after LI-rTMS.

Values are mean ± SD. No significant difference was found between the pre- and post-stimulation (P1) period (n = 8 neurons; paired Student t-test; $P > 0.16$ for each parameter).